

When Feedback Fails: The Scaling and Saturation of Star Formation Efficiency

Michael Y. Grudić^{★1}, Philip F. Hopkins¹, Claude-André Faucher-Giguère², Eliot Quataert³, Norman Murray^{4,5}, Dušan Kereš⁶

¹TAPIR, Mailcode 350-17, California Institute of Technology, Pasadena, CA 91125, USA

²Department of Physics and Astronomy and CIERA, Northwestern University, 2145 Sheridan Road, Evanston, IL 60208, USA

³Department of Astronomy and Theoretical Astrophysics Center, University of California Berkeley, Berkeley, CA 94720

⁴Canadian Institute for Theoretical Astrophysics, 60 St. George Street, University of Toronto, ON M5S 3H8, Canada

⁵Canada Research Chair in Astrophysics

⁶Department of Physics, Center for Astrophysics and Space Science, UC San Diego, 9500 Gilman Drive, La Jolla, CA 92093

Submitted to MNRAS, December, 2016

ABSTRACT

We present a suite of 3D multi-physics MHD simulations following star formation in isolated turbulent molecular gas disks ranging from 5 to 500 parsecs in radius. These simulations are designed to survey the range of surface densities between those typical of Milky Way GMCs ($\sim 10^2 \text{ M}_\odot \text{ pc}^{-2}$) and extreme ULIRG environments ($\sim 10^4 \text{ M}_\odot \text{ pc}^{-2}$) so as to map out the scaling of star formation efficiency (SFE) between these two regimes. The simulations include prescriptions for supernova, stellar wind, and radiative feedback, which we find to be essential in determining both the instantaneous (ϵ_{ff}) and integrated (ϵ_{int}) star formation efficiencies. In all simulations, the gas disks form stars until a critical stellar surface density has been reached and the remaining gas is blown out by stellar feedback. We find that surface density is a good predictor of ϵ_{int} , as suggested by analytic force balance arguments from previous works. Furthermore, SFE eventually saturates to a fraction of order unity at high surface density. We also find a proportional relationship between ϵ_{ff} and ϵ_{int} , implying that star formation is feedback-moderated even over very short time-scales in isolated clouds. These results have implications for star formation in galactic disks, the nature and fate of nuclear starbursts, and the formation of bound star clusters. The scaling with surface density of ϵ_{ff} conflicts with the notion that ϵ_{ff} is always $\sim 1\%$ on the scale of GMCs, but our predictions do recover the $\sim 1\%$ value for typical local GMCs with $\Sigma_{gas} \sim 100 \text{ M}_\odot \text{ pc}^{-2}$.

Key words: galaxies: star formation — galaxies: starburst — galaxies: active — galaxies: nuclei — galaxies: star clusters: general

1 INTRODUCTION

Typically, star formation in the observed Universe is inefficient. Star formation is observed to occur in giant molecular clouds (GMCs) formed in galactic disks, and the per-freefall star formation efficiency of a star-forming region may be parametrized as:

$$\dot{M}_\star(t) = \epsilon_{ff}(t) \frac{M_{gas}(t)}{t_{ff}(t)}, \quad (1)$$

where \dot{M}_\star is the star formation rate, M_{gas} is the gas mass “available” to form stars (observationally, the mass of molecular gas as obtained from a tracer such as CO or HCN), and $t_{ff}(t)$ is the local gravitational freefall time. ϵ_{ff} is the fraction of available gas converted to stars per t_{ff} ; on galac-

tic ($\sim \text{kpc}$) scales, ϵ_{ff} has been estimated by fitting to the relation:

$$\Sigma_{SFR} = \epsilon_{ff}^{gal} \Sigma_{gas} t_{ff}^{-1}, \quad (2)$$

where Σ_{SFR} is the projected density of star formation in the disk, Σ_{gas} is the projected (cold) gas density, t_{ff} is the local freefall time evaluated from the galaxy’s scale height-averaged density, and ϵ_{ff}^{gal} has been found to be ~ 0.02 (Kennicutt 1998). Thus, a typical galaxy converts only 2% of its potentially star-forming gas into stars each freefall time, despite the tendency of self-gravitating cold gas clouds to fragment and contract nearly all of their gas mass to high densities within only a few t_{ff} . Clearly, some physical mechanism is responsible for the moderation of star formation.

Recently, the FIRE¹ (Feedback In Realistic Environ-

[★] E-mail: mgrudich@caltech.edu

¹ <http://fire.northwestern.edu>

ments) simulations (Hopkins et al. 2014, 2017) have demonstrated that the inefficiency of star formation in galaxies formed within the Λ CDM cosmology can be explained by stellar feedback alone, obtaining good agreement with Kennicutt (1998) independent of the numerical resolution-scale star formation model. As stars form in dense GMCs within a galaxy, some combination of photoionization heating, radiation pressure, stellar winds, and possibly supernovae blow out the remaining gas in the cloud, terminating star formation locally. The gas ejecta and the young stars formed inject momentum into the surrounding ISM, which prevents the runaway vertical collapse of the galactic disk by providing turbulent support, and the rates of turbulent dissipation and momentum injection are in equilibrium when $\epsilon_{ff}^{gal} \sim 0.02$ (see Thompson et al. (2005); Ostriker & Shetty (2011); Faucher-Giguère et al. (2013); Orr et al. (2017)).

However, this mechanism only explains the rate of star formation on galactic scales: ϵ_{ff}^{gal} emerges from an established equilibrium over the formation and disruption of many GMCs, and is distinct from the value of ϵ_{ff} for a single GMC. Since star formation in a GMC must cease once it is disrupted, there exists another quantity of interest in characterizing the efficiency of star formation, the integrated SFE:

$$\epsilon_{int} = \frac{M_{\star}}{M_{tot}}, \quad (3)$$

where M_{\star} is the final mass of stars formed and M_{tot} is the mass of the initial gas cloud. In Milky Way GMCs, the median value of ϵ_{int} is ~ 0.03 , with a large observed scatter of 0.8 dex (Murray 2011; Lee et al. 2016). However, there is evidence that ϵ_{int} is much higher in denser conditions: Murray et al. (2010) points out that the masses of GMCs (Keto et al. 2005) and young star clusters (McCraday & Graham 2007) in the M82 starburst galaxy are of a similar scale, suggesting that ϵ_{int} is of order unity at the greater surface densities of such regions. Indeed, the existence of young, bound star clusters *in general* may physically require high integrated SFE on at least some local scale (Hills 1980; Elmegreen & Efremov 1997). Recent observations of young massive clusters have also suggested a time constraint of < 4 Myr for cluster formation within the disk of M83 (Hollyhead et al. 2015), suggesting that cluster formation may also be rather fast ($\epsilon_{ff} \sim 1$). Therefore, it is necessary to explore ways in which the efficiency of star formation, both in terms of ϵ_{ff} and ϵ_{int} , can scale from Milky Way-like values of $\sim 1\%$ to greater values. Since stellar feedback is responsible for the eventual disruption of molecular clouds against gravity, it is likely that the balance of these two forces plays a major role in determining both the speed and integrated efficiency of star formation below kpc scales.

In this paper, we focus on the detailed behaviour of a single star formation episode at high resolution: we present 3D MHD simulations of star-forming gas disks which use the numerical treatments of cooling, star formation and stellar feedback of Hopkins et al. (2017) to answer certain basic questions about star formation in local galactic environments:

- Given an initial self-gravitating gas distribution, what is the resulting star formation history? In particular, what

determines the observable quantities ϵ_{ff} and ϵ_{int} , and how are they related?

- How do the initial parameters of the gas cloud map onto the properties of the formed stellar system?
- Which physical mechanisms have the greatest effect upon the answers to these questions?

The general approach of this study is to suppose some generic initial conditions for an isolated gas disk, neglecting its interaction with the surrounding galactic environment. This approximation makes sense for simulations spanning no more than a few dynamical times (which we shall show to be the case) and allows us to achieve relatively high spatial and mass resolution in the region of interest for modest computational cost.

This physics problem is most conventionally applicable to star-forming GMCs, but really any region in which the dynamical time is not significantly longer than the main sequence lifetime of massive stars (~ 3 Myr) should be unstable to runaway star formation and the eventual blowout of the gas component (Torrey et al. 2016). The central regions of ultraluminous infrared galaxies (ULIRGs) often have large gas fractions and short dynamical times (Downes & Solomon 1998; Bryant & Scoville 1999), so for the purposes of our problem they may effectively behave as one super-GMC with particularly high ($> 10^3 M_{\odot} \text{pc}^{-2}$) surface density. Our simulations, which probe these surface densities, can therefore also serve as models of gas-rich nuclear disks, which host the most extreme star formation events in the local Universe.

This paper is structured as follows: in Section 2, we describe a simple model of a gas-rich, star-forming disk, and predict its general behaviour from the physical arguments. In Section 3, we describe the methods for our simulations, their initial conditions, and the scope of our survey of physics and simulation parameters. In Section 4 we present the results of the simulations concerning the global properties of the star-forming clouds: the overall behaviour of the simulated clouds, the isolated effects of various physical mechanisms, the per-freefall (ϵ_{ff}) and integrated (ϵ_{int}) star formation efficiency. Finally, in Section 5 we discuss some applications, implications and limitations of our results and outline future studies on the more detailed aspects of the mode of star formation we have simulated.

2 A STAR-FORMING DISK MODEL

To guide the methodology of the numerical study, we first review some basic theory of star formation and construct a simple model that captures the basic physics of how feedback determines the SFE of a gas-rich star-forming disk over < 3 Myr dynamical times. Consider an initially-uniform disk of mass M , radius R , and scale height h that initially consists of only gas. Averaged over the diameter of the disk, the initial surface density is then:

$$\Sigma_{tot,0} = \Sigma_{gas}(t=0) = \frac{M}{\pi R^2}. \quad (4)$$

2.1 time-scales for star formation

The longest possible time-scale for gravitational collapse within the disk is the freefall time $t_{ff,0}$ derived from the

system's physical parameters M and R :

$$t_{ff,0} = \frac{\pi}{2} \sqrt{\frac{R^3}{2GM}} = 2 \text{ Myr} \left(\frac{R}{50 \text{ pc}} \right)^{\frac{3}{2}} \left(\frac{\Sigma_{tot,0}}{10^3 M_{\odot} \text{ pc}^{-2}} \right)^{-\frac{1}{2}}, \quad (5)$$

which is proportional to the outer orbital period of the disk. This is the longest relevant time-scale in the problem, since we neglect environmental interactions. $t_{ff,0}$ may overestimate the typical gravitational collapse time of a typical gas parcel, as we expect that if star formation is to occur then there will be hierarchical turbulent fragmentation driving mass to greater-than-average densities. Specifically, isothermal, self-gravitating turbulence has been found to produce a density PDF with a high-density power-law tail due to gravity (Kritsuk et al. 2011), and at lower densities a log-normal form, as emerges in isothermal turbulence without gravity (Vazquez-Semadeni 1994; Padoan et al. 1997; Nordlund & Padoan 1999). The only characteristic density is the peak of this distribution, so we define a shorter freefall time in terms of the median gas density ρ_{50} ²:

$$t_{ff,50} = \sqrt{\frac{3\pi}{32G\rho_{50}}} = 1.6 \text{ Myr} \left(\frac{n_{50}}{10^3 \text{ cm}^{-3}} \right)^{-\frac{1}{2}}, \quad (6)$$

where n_{50} is the median particle number density. $t_{ff,50}$ will generally be a more reasonable unit for the gas depletion time, and hence for comparing values of ϵ_{ff} .

In the parameter space relevant to star formation in the local Universe, the cooling time of gas that is metal-enriched or molecular is generally much less than both $t_{ff,0}$ and $t_{ff,50}$. Therefore, in absence of stars or external inputs, any thermal energy supporting against self-gravity will quickly radiate away. If the disk has some initial turbulent velocity dispersion, that energy too will be cooled away by shocks over $\sim t_{ff,50}$. Without some imposed stabilizing force the disk will be subject to gravitational instability, fragmentation, and star formation.

The process of fragmentation involves a runaway collapse to protostellar densities. If an initially-smooth disk with $\rho \sim \Sigma_{tot,0}/2h$ were to fragment hierarchically into successively denser structures, the entire conversion of gas into stars would take no longer than a time on the order of $\sim t_{ff,50}$, since the freefall time at all smaller scales is less than this. Counting the time for the initial growth of the gravitational instability, we therefore expect the entire period of star formation to last no longer than several freefall times. This appears to be the case for Milky Way GMCs (Murray 2011; Lee et al. 2016) as well as those found in simulated galaxies with low-temperature cooling and stellar feedback (Hopkins et al. 2012a).

² Note that we use the median, and not the mass-weighted mean gas density used for determining t_{ff} in Krumholz et al. (2011) and Myers et al. (2014). The mass-weighted mean is less suitable for estimating t_{ff} in the middle of star formation because the high-density power-law tail in the density PDF biases it toward high densities. We also find that it is not robust with respect to simulation resolution, as higher resolutions will resolve more of the power-law tail. The median density generally lies near the peak of the density PDF, and is robust with respect to resolution.

2.2 Star Formation Efficiency

As stars form, the stellar surface density $\Sigma_{\star}(t)$ increases as the gas surface density $\Sigma_{gas}(t) = \Sigma_{tot,0} - \Sigma_{\star}(t)$ decreases. These stars will inject energy and momentum into the gas through various feedback mechanisms, however if the time-scale of star formation is so short that SNe do not occur then direct ISM heating can be neglected due to the short cooling time. Assuming that the stellar population is well-sampled from a Kroupa (2002) IMF, the rate of momentum feedback injection per unit stellar mass $\frac{\dot{P}_{\star}}{m_{\star}}$ will initially be roughly constant, dominated by radiation pressure and fast winds from the most massive stars for the first 3 Myr after the stellar population forms. For the subsequent ~ 40 Myr, the massive stars all leave the main sequence and supernovae become the dominant form of feedback. Because we are most interested in the limit of dense systems with short dynamical times, we can neglect stellar evolution and approximate $\frac{\dot{P}_{\star}}{m_{\star}}$ as being constant. Then the force of feedback upon the gas in the disk is:

$$F_{fb}(t) = \frac{\dot{P}_{\star}}{m_{\star}} M_{\star} = \frac{\dot{P}_{\star}}{m_{\star}} \Sigma_{\star}(t) \pi R^2, \quad (7)$$

assuming no leakage, photon trapping, or other effects arising from clumpy structure. As described in Murray et al. (2010) and Torrey et al. (2016), this force will continue to increase until F_{fb} exceeds the force of gravity binding the gas to the disk. The majority of the new star formation will occur in a thin disk, so while the gas is dense enough to form stars the gravitational field binding gas to the star-forming region will be dominated by contributions from the gas itself and the newly-formed stars. Thus:

$$F_g(t) = g M_{gas}(t) = 2\pi G \Sigma_{tot,0} \Sigma_{gas}(t) \pi R^2. \quad (8)$$

By equating the force of feedback upon the gas (7) with that of gravity (8) we can determine the final stellar mass and hence the integrated star formation efficiency:

$$\epsilon_{int} = \frac{M_{\star}}{M} = \frac{\Sigma_{tot,0}}{\Sigma_{tot,0} + \Sigma_{crit}}, \quad (9)$$

where:

$$\Sigma_{crit} = \frac{1}{2\pi G} \frac{\dot{P}_{\star}}{m_{\star}} \quad (10)$$

is the quantity with units of surface density encoding the strength of feedback relative to gravity. The contributions to $\frac{\dot{P}_{\star}}{m_{\star}}$ from single-scattering radiation pressure, stellar winds, and SNe ejecta (ignoring the work done in the energy-conserving phase) are all of order $10^3 \frac{L_{\odot}}{M_{\odot} c}$. Thus, $\Sigma_{crit} \sim 10^{3-4} M_{\odot} \text{ pc}^{-2}$ due to stellar feedback physics. Observationally, the median ϵ_{int} for Milky Way GMCs is $\sim 3\%$ (Murray 2011; Lee et al. 2016), while the median GMC surface density is $\sim 100 M_{\odot} \text{ pc}^{-2}$ (Larson 1981; Solomon et al. 1987; Bolatto et al. 2008), so we can estimate that $\Sigma_{crit} = 3000 M_{\odot} \text{ pc}^{-2}$ for these GMCs.

Equation (9) implies that the efficiency of starbursts occurring over adequately short time-scales is simply dictated by the ratio of forces of feedback and gravitation. In the limit $\Sigma_{tot,0} \ll \Sigma_{crit}$, SFE is proportional to $\epsilon_{int} \propto \Sigma_{tot,0}$ with the constant of proportionality determined by the strength of feedback. Inversely, where $\Sigma_{tot,0} \gg \Sigma_{crit}$, SFE should approach unity: gravity prevails against feedback and converts nearly all gas to stars.

The corresponding result for any other geometry or mass profile would be identical except that Σ_{crit} would differ by a factor of order unity (see Fall et al. (2010), Murray et al. (2010), Dekel & Krumholz (2013), and Thompson & Krumholz (2016) for similar derivations with various cloud and feedback models). The importance of surface density in determining star formation efficiency in short dynamical time systems is not simply a consequence of the ‘diskiness’ of star-forming systems, nor of their optical depth in some band, both of which would give surface density an obvious physical relevance. It is merely a consequence of the fact that the ratio between the force of self gravity $F_g \sim \frac{GM^2}{R^2}$ and the momentum injection rate of feedback $F_{fb} \sim M_\star \dot{P}_\star / m_\star$ has dimensions of surface density, at least under our simplifying assumptions.

2.3 Cluster formation

The quantity ϵ_{int} is likely to be the determining parameter for the formation of bound clusters from gas (Hills 1980). Assuming that a star cluster is close to virial equilibrium at the time it blows out its natal cloud, simple estimates require that $\epsilon_{int} > 1/2$ if the stellar system is to remain bound. It is therefore expected that the cluster formation efficiency, the fraction of stars found in bound clusters, is a function of ϵ_{int} , and hence of $\Sigma_{tot,0}$ by equation 9. If equation 9 holds, then cluster formation should be generic to regions of high Σ_{gas} . And indeed, rich populations of young bound clusters are ubiquitous in dense nuclear starbursts, including notable examples Arp 220 (Wilson et al. 2006), M82 (McCraday & Graham 2007), and M83 (Bastian et al. 2012; Ryon et al. 2015).

This is not to say that bound cluster formation cannot take place in star formation events with $\epsilon_{int} \ll 0.5$ on average. To the contrary, GMCs in the Milky Way and other nearby galaxies typically have $\Sigma_{gas} \sim 100 M_\odot \text{pc}^{-2}$ (Larson 1981; Solomon et al. 1987; Bolatto et al. 2008), giving $\epsilon_{int} \sim 3\%$ at best, yet young bound star clusters are still observed to have formed within the galaxy (Portegies Zwart et al. 2010). Rather than simply turning off below a certain surface density threshold, the bound cluster formation efficiency appears to scale smoothly as a function of Σ_{gas} , saturating to a value of $\sim 70\%$ (Kruijssen 2012). Star cluster formation may be possible in environments that are less dense on average because star-forming clouds are hierarchically structured, with a broad, nominally log-normal³ surface density PDF. If ϵ_{int} is determined in a scale-free fashion according to equation 9, it will apply just as well on the scale of denser-than-average subclouds once they decouple from their environment, allowing them to have high ϵ_{int} locally even if ϵ_{int} is small on larger scales (e.g. Kruijssen et al. (2012)). If this argument is valid, we expect to see bound cluster formation in any star-forming disk in which there is enough gas mass to sample an underlying cluster mass function.

³ Neglecting the high-density tail from gravitationally collapsing regions, as proposed by Kritsuk et al. (2011).

3 SIMULATIONS

Our simulations use GIZMO (Hopkins 2015)⁴, a mesh-free, Lagrangian finite-volume Godunov code designed to capture advantages of both grid-based and smoothed-particle hydrodynamics (SPH) methods, built on the gravity solver and domain decomposition algorithms of GADGET-3 (Springel 2005). In Hopkins (2015) and Hopkins & Raives (2016) we consider extensive surveys of test problems in both hydrodynamics and MHD, and demonstrate accuracy and convergence in good agreement with well-studied regular-mesh finite-volume Godunov methods and moving-mesh codes (e.g. ATHENA & AREPO; Stone et al. 2008; Springel 2010). We run GIZMO in its Meshless-Finite Mass (MFM) mode but have verified that Meshless Finite-Volume (MFV) mode produces nearly identical results (as expected from the previous studies).

3.1 Cooling, Star Formation, and Stellar Feedback

The simulations here use the physical models for star formation and stellar feedback developed for the Feedback In Realistic Environments (FIRE) project (Hopkins et al. 2014, 2017), although the simulations in this paper are idealized cloud collapse experiments on small scales, at often much higher mass resolution than the FIRE simulations. In general, we expect these methods to be appropriate to the scales examined in this work because by construction the FIRE framework adopts a physics approach that requires no phenomenological tuning to different mass scales. Hydrodynamics, gravity, cooling, and stellar feedback are explicitly and approximately solved down to the resolution limit, and the physics approximations invoked have been extensively validated by more expensive and detailed simulations. We briefly summarize some key properties of the FIRE models here, but refer to Hopkins et al. (2017) for details of the numerical implementations and extensive tests of the algorithms and physics.

It is critical for understanding gas fragmentation to have explicit cooling physics; we therefore do *not* adopt an “effective equation of state” (Springel & Hernquist 2003) as has been done in many works in the past, but explicitly follow a wide range of heating/cooling processes. This includes photo-ionization and photo-electric, dust collisional, Compton, metal-line, molecular, and fine-structure processes, and we self-consistently account for optically thick cooling when local regions become thick to their own cooling radiation, implementing the approximation of Rafikov (2007). We do neglect the effects of non-equilibrium chemistry in the ISM, which can be very important for predictions of observational tracer abundances (Richings et al. 2014a,b), however cooling times are generally so short in our problem that little dynamical effect can be expected.

Gas particles are converted to star particles stochastically if they satisfy all of the following star formation criteria:

- *Self-shielding and molecular*: We compute the molecular fraction f_{mol} of the gas as a function of column density

⁴ A public version of this code is available at www.tapir.caltech.edu/~phopkins/Site/GIZMO.html.

and metallicity according to [Krumholz & Gnedin \(2011\)](#), estimating the local gas column density with a Sobolev approximation.

- *Contracting*: Star formation occurs only in regions of increasing density ($\nabla \cdot \vec{v} < 0$).
- *Self-gravitating*: The local Jeans mass M_{jeans} is estimated, accounting for both turbulent ([Hopkins et al. 2013](#)) and thermal contributions, with the turbulent contribution typically dominating in cold molecular gas. Star formation is allowed only in regions where the Jeans mass can no longer be resolved, as it is at this point that fragmentation should continue down to unresolved scales.

In tests, we find that the self-gravity criterion is the most restrictive and the most physically motivated of the above. Note that these are criteria are slightly different from the cosmological simulations of [Hopkins et al. \(2014\)](#) and [Hopkins et al. \(2017\)](#), as we do not enforce a threshold density for star formation. All star formation criteria are fully adaptive, with no built-in scales that could be imprinted upon the star clusters that form. To summarize, gas fragmentation is explicitly followed down to the scale where the mass resolution is insufficient, then the gas particles quickly (within one local t_{ff}) transition into collisionless star particles.

Crucially, because the collapse time-scale of *resolved* fragments at densities much larger than the mean in our simulations is always fast compared to the global dynamical time, this is not the rate-limiting step for star formation. Rather, it is the initial formation of these fragments ([Thompson et al. 2005](#); [Faucher-Giguère et al. 2013](#); [Ostriker & Shetty 2011](#)). As such, we will show that the star formation histories are insensitive to details of both our cooling and star formation prescriptions. This is consistent with a wide range of previous studies on GMC and galactic scales ([Saitoh et al. 2008](#); [Hopkins et al. 2011, 2012a,b, 2016, 2017](#); [Agertz et al. 2013](#)).

Once stars form, feedback is included in the form of radiation pressure (UV, optical, and IR), stellar winds (fast, young star winds and slow AGB winds), SNe (types Ia and II), photo-ionization and photo-electric heating. Every star particle is treated as a single stellar population with an age based on its formation time and metallicity and mass inherited from its parent gas particle. Feedback includes the relevant mass, metal (with 11 separately tracked species), momentum, and energy injection to the neighboring gas; all of the relevant quantities (stellar luminosities, spectral shapes, SNe rates, wind mechanical luminosities, yields) for the mechanisms above are tabulated as a function of time directly from the stellar population models in STARBURST99, assuming a [Kroupa \(2002\)](#) IMF. For SNe, if we lack the mass resolution to resolve the Sedov-Taylor phase, we estimate the work done during the energy-conserving phase and couple the appropriate momentum based on fits from high-resolution SNR simulations ([Martizzi et al. \(2015\)](#); [Kim & Ostriker \(2015\)](#), see [Hopkins et al. \(2014\)](#) for implementation details). This is only important for our few simulations with resolved masses greater than $10^3 M_{\odot}$.

For the multi-band radiative fluxes necessary for the radiative heating and pressure terms, we use the LEBRON approximation, described in detail in [Hopkins et al. \(2017\)](#). The spectrum is binned into ionizing, far-UV, near-UV, optical/near-IR, and mid/far-IR bands, and the approxi-

mate fluxes are computed explicitly at each particle. We emphasize that, unlike the model of [Hopkins et al. \(2012a\)](#), LEBRON does not invoke a subgrid “boost” term for the radiation pressure of multiply-scattered IR photons. Only explicitly-resolved absorption is accounted for in the heating and pressure terms.

We intentionally assign IMF-averaged properties to all star particles, rather than attempting to follow individual stars explicitly – our goal is to study the effects of feedback, given some IMF, *not* to solve the problem of the origins and nature of the IMF itself. The latter would require a full model for individual star formation (and much higher resolution than we are able to achieve here), and may critically depend on additional physics (e.g. heating by protostellar accretion, protostellar jets) which are negligible in an IMF-averaged feedback scenario.⁵ In some of our less-massive simulated clouds, the particle mass is less than M_{\odot} and the stellar IMF is nominally resolvable, so star formation tends to produce “clusters” of star particles of $100M_{\odot}$ or less, which can be identified with the individual stars that would have formed. In this case, a sink-particle method (e.g. [Bate et al. \(1995\)](#)) is certainly much more realistic and efficient, however we still adopt the standard star-particle method for consistency with the more massive clouds.

3.2 Initial Conditions & Problem Setup

The initial conditions of the simulations consist of a constant density gas sphere of radius R and mass M , with the parameter space of R and M tabulated in table 1. These values are chosen to cover a range of values of $\Sigma_{\text{tot},0}$, which, for reasons discussed in Section 2, we expect to roughly parametrize the overall behaviour of the system even at disparate spatial scales, masses, and dynamical times.

The initial velocity field is a superposition of solid-body rotation about the origin and a random turbulent component. The rotational frequency is set to the gas ball’s Keplerian frequency $\Omega_K = (GM/R^3)^{1/2}$, so that the effective radius, and hence average surface density of the disk remains roughly constant⁶. The random velocity component adds

⁵ One might worry that, by IMF-averaging, we make feedback “too smooth.” In limited experiments, we have crudely modeled the effects of stochastic sampling of the IMF and concentrating feedback in individual massive stars by, for each star particle, drawing from the IMF a quantized number of massive O-stars (from a Poisson distribution with mean equal to the expectation for the total mass of the particle). All feedback effects associated with massive stars (Type-II SNe, photo-heating, fast winds, radiation pressure) are multiplied appropriately by the number of O-stars (which are lost in each Type-II SNe event). As expected, this has essentially no effect on the disk-averaged properties we consider here for disk masses $\gtrsim 1000 M_{\odot}$, which reasonably sample massive ($\gtrsim 10 M_{\odot}$) stars. For still smaller clouds, this (as expected) introduces additional scatter in the star formation efficiency, corresponding to the variation in the number of massive stars (hence strength of feedback). However, the mean scalings are unaffected.

⁶ Note that assuming rotational support is not a realistic choice for simulating GMCs, which are generally supported by a shearing velocity gradient and turbulence. As such, the simulations are not expected to result in large-scale cloud morphologies resembling realistic galactic GMCs. However, the morphology of

Simulation parameters

$\Sigma_{tot,0}$ [$M_{\odot} \text{pc}^{-2}$] (1)	R [pc] (2)	M [M_{\odot}] (3)	$t_{ff,0}$ [Myr] (4)	Modifications (5)	Mass Resolution [M_{\odot}] (6)	Minimum star particle softening [pc] (7)
127	5	10^4	1.85		0.03	0.001
127	50	10^6	5.86		3	0.01
127	500	10^8	18.53		300	0.1
382	5	3×10^4	1.07		0.03	0.001
382	50	3×10^6	3.38		3	0.01
382	500	3×10^8	10.70		300	0.1
1270	5	10^5	0.59		0.1	0.001
1270	50	10^7	1.85	“Standard”	10	0.01
1270	50	10^7	1.85	Random IC seeding 2	10	0.01
1270	50	10^7	1.85	Random IC seeding 3	10	0.01
1270	50	10^7	1.85	Optically-thin cooling	10	0.01
1270	50	10^7	1.85	No feedback	10	0.01
1270	50	10^7	1.85	1/2-strength feedback	10	0.01
1270	50	10^7	1.85	$\times 2$ -strength feedback	10	0.01
1270	50	10^7	1.85	Radiation pressure only	10	0.01
1270	50	10^7	1.85	150^3 particle resolution	2.96	0.01
1270	50	10^7	1.85	50^3 particle resolution	80	0.01
1270	50	10^7	1.85	1% local SFR	10	0.01
1270	50	10^7	1.85	$0.01Z_{\odot}$ initial metallicity	10	0.01
1270	500	10^9	5.86		1000	0.1
3820	5	3×10^5	0.34		0.3	0.001
3820	50	3×10^7	1.07		30	0.01
3820	500	3×10^9	3.38		3000	0.1
12700	5	10^6	0.19		1	0.001
12700	50	10^8	0.59		100	0.01
12700	500	10^{10}	1.85		10000	0.1

Table 1. Initial conditions, numerical parameters and modifications of the simulations in this paper: (1): $\Sigma_{tot,0}$: the initial average gas surface density in $M_{\odot} \text{pc}^{-2}$. (2): R : the radius of the initial spherical gas cloud in pc. (3): M : the initial gas mass in M_{\odot} . (4): The freefall time $t_{ff,0}$ at the initial density, defined in equation 5. (5): Modifications to the simulation with respect to the standard setup described in Section 3. (6): Particle mass resolution in M_{\odot} . (7) Minimum Plummer-equivalent force softening for star particles. No minimum softening for gas particles is imposed. The particle number is 100^3 in all simulations unless otherwise specified. All simulations start with solar metal abundances (except where stated otherwise), and an initial temperature of 10^4 K.

a turbulent energy of 10% of the initial gravitational binding energy, with a power spectrum $E(k) \propto k^{-2}$. All velocity Fourier coefficients for which $\|\vec{k}\| \geq \frac{2\pi}{R}$ are given a random phase and scaled according to this relation. The velocity components are first computed on a Cartesian grid circumscribing the gas sphere, and are then interpolated to the particle positions.

The seed magnetic field is constructed in a similar fashion, such that the power spectrum of magnetic energy is also proportional to k^{-2} . The only difference from the above is that the $\nabla \cdot \vec{B}$ constraint is enforced by first computing random Fourier coefficients for the magnetic potential \tilde{A} and then applying the curl operator in Fourier space before transforming to real space in the same fashion as the velocity. The total magnetic energy is 1% of the gravitational binding energy, which is 10% of the initial turbulent energy. This figure was chosen based upon observations suggesting

sub-clouds will be determined on much shorter time-scales by local turbulence and self-gravity, independently of the large-scale morphology.

that MHD turbulence in GMCs is super-Alfvénic (Troland & Crutcher 2008), supported by high-resolution MHD simulations showing that the supersonic turbulent MHD dynamo tends to saturate the magnetic energy to 1 – 10% of the turbulent energy (Federrath et al. 2014).

The gas is initialized to a temperature of 10^4 K, however the simulations’ results are insensitive to this choice because the cooling time in all cases considered is orders of magnitude shorter than the dynamical time-scale. At the beginning of the simulation, the gas immediately cools rapidly to several tens of K, as is typical of the cold, neutral phase of the interstellar medium.

All simulations except those noted in table 1 have 10^6 particles, giving a fixed mass resolution of $10^{-6}M$. As discussed in Appendix A, the star formation histories of the simulations are insensitive to our mass resolution at or above this level.

Global simulation results

$\Sigma_{tot,0}$ [$M_{\odot}\text{pc}^{-2}$]	R [pc]	Modifications	ϵ_{int}	T_{SF} [Myr]	$T_{SF}/t_{ff,0}$	$T_{2\sigma}$ [Myr]	$T_{2\sigma}/t_{ff,0}$	$\langle\epsilon_{ff,50}\rangle_t$	$\sigma_{\log\epsilon_{ff,50}}$ [dex]
(1)	(2)	(3)	(4)	(5)	(6)	(7)	(8)	(9)	(10)
127	5		0.04	1.34	0.72	1.75	0.94	0.02	0.34
127	50		0.04	7.19	1.23	8.83	1.51	0.02	0.56
127	500		0.06	25.50	1.38	35.20	1.90	0.01	0.55
382	5		0.11	0.95	0.89	1.16	1.09	0.09	0.70
382	50		0.10	4.23	1.25	5.04	1.49	0.07	0.42
382	500		0.11	12.02	1.12	18.06	1.69	0.04	0.61
1270	5		0.31	0.77	1.31	0.81	1.38	0.11	0.77
1270	50	“Standard”	0.32	2.22	1.20	2.45	1.32	0.12	0.79
1270	50	No Magnetic Field	0.34	2.44	1.31	2.57	1.39	0.08	0.74
1270	50	Strong Magnetic Field	0.30	2.33	1.26	2.59	1.40	0.11	0.66
1270	50	No feedback	0.86+	3.25+	1.75+	3.59+	1.94+	0.52	0.62
1270	50	1/2 strength feedback	0.52	2.53	1.36	2.77	1.50	0.18	0.56
1270	50	$\times 2$ strength feedback	0.19	2.54	1.37	2.63	1.42	0.10	0.57
1270	50	Radiation pressure only	0.36	2.49	1.34	2.59	1.4	0.10	0.85
1270	50	Optically-thin cooling	0.32	2.23	1.20	2.43	1.31	0.13	0.54
1270	50	Slow subgrid SFR	0.30	1.79	0.97	1.85	1.00	0.11	1.03
1270	50	$Z = 10^{-2}Z_{\odot}$	0.35	2.05	1.11	2.13	1.15	0.14	0.75
1270	50	Random Seeding 2	0.30	2.06	1.11	2.32	1.25	0.11	0.56
1270	50	Random Seeding 3	0.28	2.03	1.10	2.23	1.20	0.10	0.63
1270	50	150^3 particle resolution	0.26+	1.98+	1.07+	2.12+	1.15+	0.10	0.60
1270	50	50^3 particle resolution	0.33	2.78	1.50	3.10	1.67	0.10	0.37
1270	500		0.31	7.50	1.28	7.91	1.35	0.14	0.83
3820	5		0.49	0.55	1.61	0.61	1.81	0.22	0.51
3820	50		0.51	1.58	1.48	1.73	1.62	0.29	0.48
3820	500		0.50	5.06	1.50	5.35	1.58	0.33	0.50
12700	5		0.63	0.33	1.76	0.36	1.95	0.20	0.50
12700	50		0.65	1.02	1.74	1.17	1.99	0.20	0.47
12700	500		0.64	3.14	1.69	3.37	1.82	0.20	0.73

Table 2. Important global quantities predicted by the simulations. Values denoted with a ‘+’ indicate a lower bound. (1-3) As Table 1. (4) ϵ_{int} , the integrated star formation efficiency (equation 3). (5) T_{SF} , the characteristic width of the peak in the star formation history (equation 12), in Myr. (6) T_{SF} in units of the initial freefall time $t_{ff,0}$. (7) $T_{2\sigma}$, the interval of time containing 95% of star formation in Myr. (8) $T_{2\sigma}$ in units of the initial freefall time $t_{ff,0}$. (9) $\langle\epsilon_{ff,50}\rangle_t$, the time-averaged per-freefall SFE defined in terms of the median gas density. (10) $\sigma_{\log\epsilon_{ff,50}}$, the dispersion in $\log\epsilon_{ff,50}$ in dex.

4 RESULTS

4.1 Overview

Qualitatively, all simulations follow the sequence of events illustrated in Figure 1. The turbulent gas cloud immediately cools, with the lowest temperatures reaching ~ 10 K. The initial velocity and magnetic fields seed density fluctuations and the gravitational instability grows, condensing the cloud into filaments and clumps. Within a freefall time, the first star clusters have formed. The star formation rate accelerates over $\sim t_{ff,0}$ to a peak value $\text{SFR}_{max} \propto \epsilon_{ff}M/t_{ff}$, with most star formation occurring in dense molecular subclouds. At this point the moderating effect of feedback comes into play and the SFR starts to drop as the disk acquires significant turbulent support. Eventually, all gas is blown out of the central region by feedback and star formation ceases (see Murray et al. (2010) and citettorrey:2016.feedback.instability for discussion of this process).

The product of the starburst is invariably a population of stars in both bound and unbound star clusters. Clusters form regardless of the overall star formation efficiency, in the

densest regions of the cloud. The trend in cluster formation efficiency predicted by Kruijssen (2012) is apparent, with the proportion of stars remaining in bound clusters increasing with $\Sigma_{tot,0}$. Because we have imposed no background potential, the mass loss of the blowout unbinds the system of clusters when $\epsilon_{int} \lesssim 50\%$, and they fly apart. At higher efficiencies, most of the clusters remain bound to each other and merge hierarchically into fewer main clusters. In a realistic scenario, the star clusters would be subject to the effects of the background stellar and dark matter distribution, which would confine the clusters to the halo potential, and possibly subject them to tidal disruption or sinking under dynamical friction. However, these effects all generally become important over multiple dynamical times after the end of star formation, which is much longer than the actual simulations.

4.2 Effects of Different Physics

In Figure 2, we compare the star formation histories of the simulations evolved from identical initial conditions but with

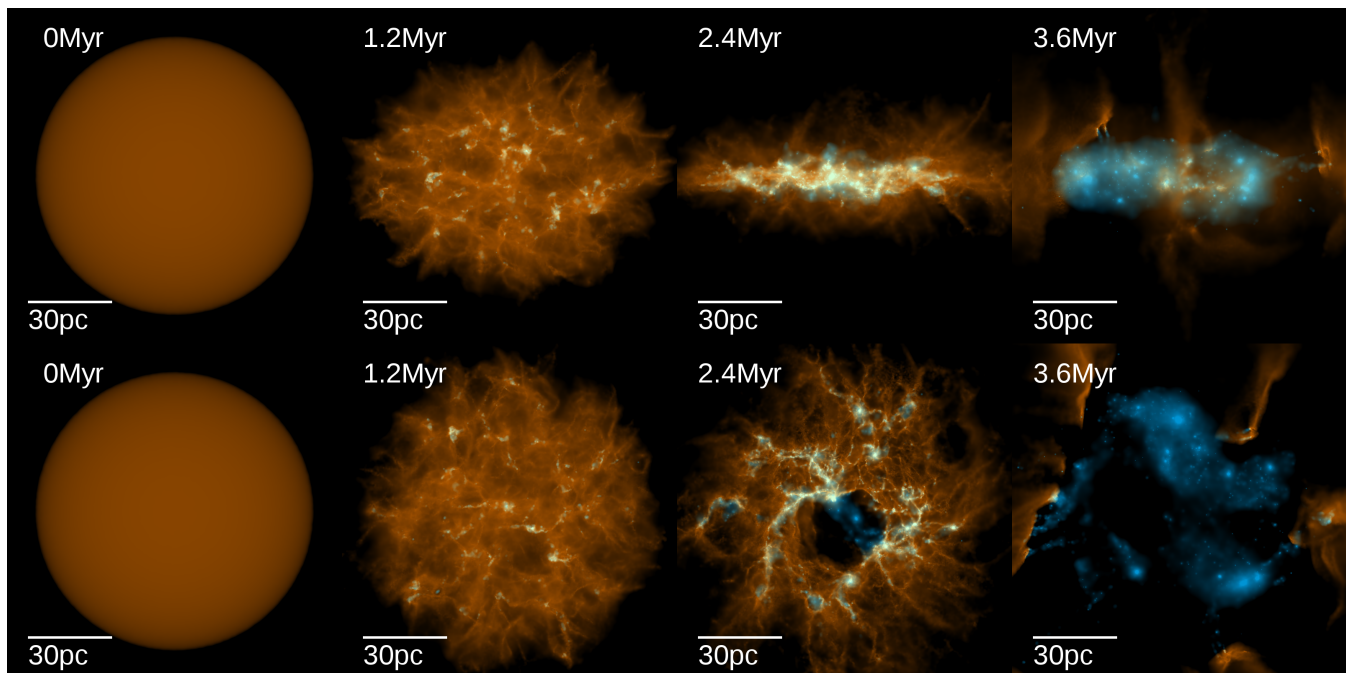


Figure 1. Surface density of gas (orange) and stars (blue) in our fiducial run with parameters $M = 3 \times 10^7 M_{\odot}$ and $R = 50$ pc, projected parallel (*top row*) and normal (*bottom row*) to the disk plane. *Far left:* The initial conditions, a uniform-density sphere. *Centre left:* After a time $\sim t_{ff,0} = 1.2$ Myr, star formation has begun. *Centre right:* After another $t_{ff,0}$ has passed, the star formation rate has peaked and large star clusters have appeared. *Far right:* The system has reached the critical stellar mass, at which point the gas is blown out of the system by feedback, evacuating the central region.

different physics enabled or disabled. It can be readily seen that the effect of varying the strength of feedback dwarfs all others, analogous to the conclusions of [Su et al. \(2016\)](#) for galaxy-scale star formation. Here we enumerate and describe these modifications and explain why, physically, this should be the case.

4.2.1 Stellar feedback

In one run, we neglect feedback altogether, and in two others we scale all energy and momentum feedback rates by $1/2$ and 2 respectively. We find that without any feedback moderation, star formation consumes nearly all (86% by the end of the simulation) gas within $\sim 2t_{ff,0}$, with no sign of stopping. If the strength of feedback is scaled by $1/2$, the star formation efficiency nearly doubles, while it is roughly halved when feedback is twice as strong. This is in agreement with equation 9. The time-scale for star formation remains unchanged, so the average per-freefall star formation efficiency ϵ_{ff} is also determined by the strength of feedback.

We also perform a run in which radiation pressure is the only feedback mechanism, and find that there is only marginally ($< 10\%$) more star formation than the standard run. Thus, radiation pressure accounts for most of the feedback budget at this point in parameter space. We expect this to be generally true in clouds where the dynamical time does not greatly exceed 3 Myr. Photoionization heating may have a significant contribution to disrupting the cloud if its escape velocity is $< 10 \text{ km s}^{-1}$ ([Dale et al. 2012](#)), but this will be the case for only a couple points in the parameter space of this paper.

It is clear from the first panel of Figure 2 that the strength of feedback does not merely set the termination time of star formation: it also limits the star formation rate in an instantaneous sense - the stronger the feedback, the lesser the peak star formation rate. The specific feedback mechanism responsible for this is radiation pressure from young massive stars, as demonstrated by the radiation-pressure-only run. The radiation pressure is able to halt accretion onto cluster-forming cores, terminating star formation locally while it is still ongoing globally. Supernova feedback does not have this instantaneous effect due to its inherent time lag after initial star formation. Although we have not simulated it, a hypothetical starburst with only supernova feedback would proceed much like the zero-feedback run for the first 3 Myr, which in this case is enough time to convert nearly all gas into stars. We therefore conclude that the early feedback mechanisms from massive stars are *crucial* in setting the efficiency of rapid star formation in the high-density, short dynamical time regime studied in this work.

4.2.2 Optically-thin cooling

In one test run, we treat all radiative cooling as optically-thin (i.e. ignoring the optically-thick cooling suppression term from [Rafikov \(2007\)](#)). This increases the cooling rate at high densities substantially. However, this has no discernible effect on the simulation results, as the opacity effects on the cooling function only become important in the suppression of fragmentation at the opacity-limited mass scale $\sim 0.01 M_{\odot}$ ([Rees 1976](#)).

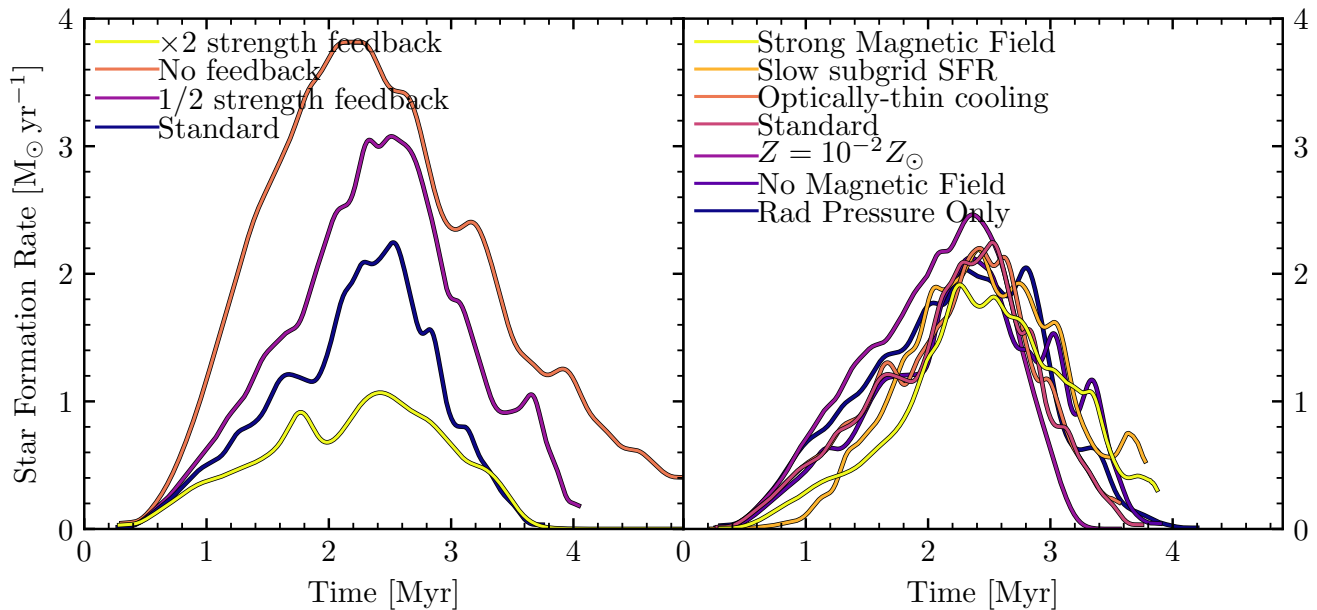


Figure 2. Star formation histories of the physics test runs using the standard initial parameters $M = 10^7 M_\odot$ and $R = 50$ pc. *Left:* Runs re-scaling the energy and momentum loadings of all stellar feedback mechanisms, producing large variations in the star formation history. *Right:* Our “standard” run compared to runs evolved from the same initial conditions with various physics options: (1) *Strong magnetic field:* Setting the initial magnetic energy to 10% of the binding energy, 10 times greater than standard. (2) *Slow subgrid SFR:* artificially “slowing” star formation in gas that satisfies the star formation criteria (Section 3.1) by multiplying the SFR by $1/100$. (3) *Optically-thin cooling:* treating all radiative cooling as optically thin. (4) $Z = 10^{-2} Z_\odot$: lowering the initial metallicity from Z_\odot to $0.01 Z_\odot$. (5) *No magnetic field:* turning off magnetic fields. (6) *Rad Pressure Only:* Removing all stellar feedback physics other than radiation pressure. These all produce relatively weak effects compared to simply rescaling the feedback energy and momentum fluxes, as discussed in section 4.2

4.2.3 Magnetic field strength

We perform a simulation with no magnetic field and a simulation with a “strong” magnetic field whose initial magnetic energy is equal to the initial turbulent energy, 10 times the standard value. A strong enough magnetic field may suppress fragmentation and the local SFR by as much as a factor of 2 on small scales (Federrath & Klessen 2012), without considering feedback. We do see this effect in the “strong” magnetic field run: the initial star formation rate is about $1/2$ that of the standard run. However, the SFR still continues to rise until it reaches the level set by feedback moderation, and the rest of the star formation history is quite similar to the other runs. Removing the magnetic field had no discernible effect upon the SFR, suggesting that the magnetic field has no large-scale dynamical relevance in the standard physics runs. However, we do note a small-scale cloud morphology in the MHD simulations that is distinctly more filamentary than the non-MHD simulation, due to the gas preferentially moving along magnetic field lines (see Collins et al. 2012).

4.2.4 Slow subgrid SFR

In this run, we force a small-scale star formation rate $\dot{\rho}_\star = 0.01 \rho_{mol} / t_{ff}$ in gas that satisfies the star formation criteria (Section 3.1). This is 100 times slower than the usual choice, and comparable to the specific star formation rate on the scale of galactic disks as measured in Kennicutt (1998). This

does not affect the average SFR in our simulations because the rate-limiting step of star formation is the formation of dense, unstable gas structures in the first place. Collections of gas particles that meet the star formation criteria but have not yet turned into stars will simply continue to contract to greater densities within a local freefall time, causing the local SFR to diverge until stars inevitably form. This result is notably different from simulations which enforce the same star formation law but do *not* follow low-temperature cooling below $10^4 K$ and adopt an effective equation of state for stellar feedback. In such a simulation, the local star formation law would underestimate the global star formation rate because the aforementioned gravitational contraction would be suppressed.

Note that this insensitivity to the local star formation efficiency is only obtained because the gas particle gravitational softening is fully adaptive. Otherwise, the cold gas would simply contract to inter-particle spacings comparable to the minimum softening and stop at that density, and the local SFR would stop increasing.

The most notable effect of this modification was the formation of much denser and much more plentiful bound star clusters. As gas exhaustion is slowed down locally, protoclusters spend more time radiating away energy, contracting, and damping out their internal turbulent motions before turning into star particles. This increases the compactness and boundedness of the remnants. We therefore caution that while global star formation histories are not sensitive to the

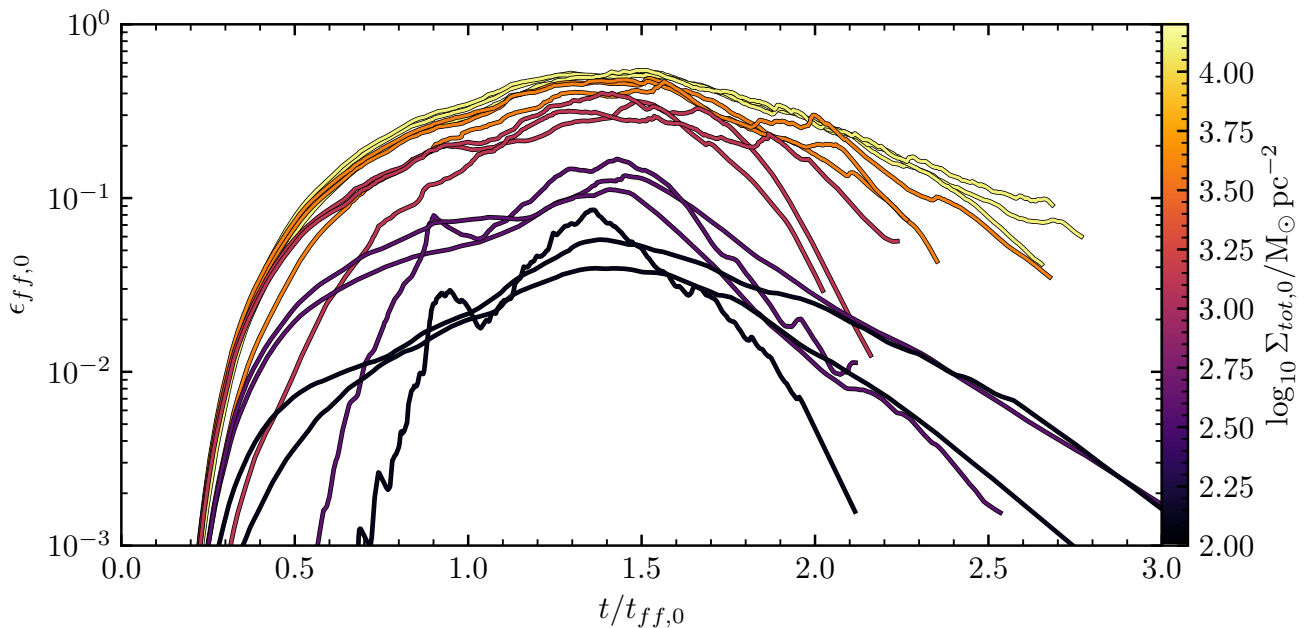


Figure 3. Dimensionless star formation histories of all parameter survey runs: the per-freefall SFE $\epsilon_{ff,0} = \frac{\dot{M}_* t_{ff,0}}{M_{gas}}$ as a function of time in units of the initial freefall time $t_{ff,0}$ for the respective run. Each curve is a single run, coloured according to the value of $\Sigma_{tot,0}$. In all cases, $\epsilon_{ff,0}$ rises to a maximum dictated by the strength of feedback relative to self-gravity, saturating to a value on the order of 1 as $\Sigma_{tot,0}$ gets large.

local value of ϵ_{ff} (see also [Hopkins et al. \(2017\)](#)), star cluster formation is.

4.2.5 Metallicity

In the low-metallicity test, we scale the initial gas metallicity down from Z_\odot to $10^{-2}Z_\odot$. This can affect many aspects of the cooling and feedback physics. Metal line cooling is proportionally less efficient, however even at $Z \sim 10^{-2}Z_\odot$, $t_{cool} \ll t_{ff}$ in the most dense gas, so fragmentation should not be strongly altered. This may change at metallicities of $10^{-4} - 10^{-5}Z_\odot$ ([Hopkins & Conroy 2015](#)). The metallicity also determines dust opacity, and thus the coupling efficiency for IR radiation pressure. Lastly, it affects the evolution of the formed stellar populations' mass, energy and momentum injection rates, which are obtained from STARBURST99. Overall, the metal-poor simulation had a star formation efficiency only marginally greater than the standard run (0.35 compared to 0.32), however it did have a faster initial growth in the SFR, suggesting that the stellar feedback at low metallicity might be less effective at halting accretion onto cluster-forming cores. The main difference in the feedback budget is due to the $\propto Z^{0.7}$ scaling of the line-driven stellar wind mass loss rate of type O stars ([Vink et al. 2001](#)). At solar metallicity, the momentum input is less radiation pressure, but within an order of magnitude. At $10^{-2}Z_\odot$, the dynamical effect is certainly negligible.

We have also performed limited experiments with our routines for cosmic ray heating, cooling, streaming and diffusion. In general, if the system is given an initial cosmic ray energy density, it will rapidly cool away into dynamical irrelevance: like the magnetic field, it is ultimately a

reservoir for the energies of gravitational collapse and stellar feedback, and not a source of energy in itself. There is also the possibility of the system being immersed in a strong cosmic ray background, however such environmental interactions are beyond the scope of this work. However, [Yoast-Hull et al. \(2016\)](#) have found that the cosmic ray energy in nuclear starbursts tends to be considerably smaller than the magnetic field energy, suggesting that even in the full picture with a realistic galactic environment cosmic rays should not greatly influence the overall dynamics of a collapsing GMC.

4.3 Integrated star formation efficiency

We now arrive at our main results. In [Figure 4](#) the star formation efficiencies of the parameter survey simulations are plotted against the surface density, escape velocity, 3D density, mass and radius derived from the simulation parameters M and R . Clearly, the mass, size, density, and escape velocity are *not* good general predictors of ϵ_{int} ; similar ϵ_{int} values are obtained in simulations for which these quantities differ by orders of magnitude.

Of the obvious physical quantities derived from M and R , $\Sigma_{tot,0}$ is the best predictor of ϵ_{int} , with particularly good agreement at high $\Sigma_{tot,0}$, where the dynamical time is always short compared to main sequence lifetimes. In general, we obtain good agreement with [equation 9](#): ϵ_{int} scales $\propto \Sigma_{tot,0}$ when $\Sigma_{tot,0} \ll \Sigma_{crit}$, and it saturates to a maximum ϵ_{int} at sufficiently high surface density. The saturation efficiency is not necessarily 1, as depends on the initial conditions and what subset of the gas is used when defining ϵ_{int} . As an extreme example, if the initial gas density field had an extended warm diffuse background component, as it might re-

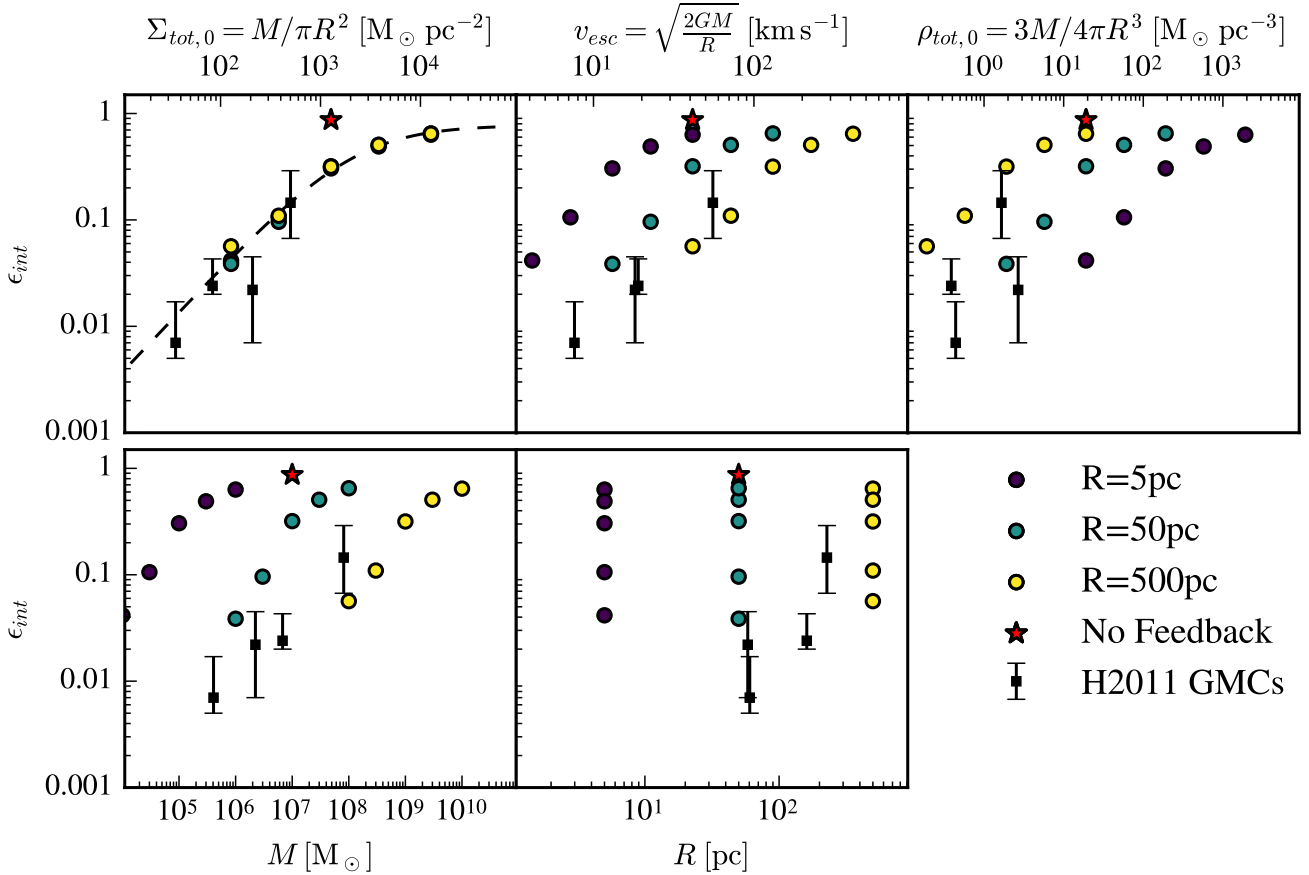


Figure 4. Integrated SFE ϵ_{int} of the 15 parameter survey simulations plotted against various functions of the initial simulation parameters M (mass) and R (radius). The points with error bars, “H2011 GMCs”, represent the populations of giant molecular clouds extracted from previous full-scale galaxy simulations (Hopkins et al. 2011). The points represent the population medians, and the bars represent the $\pm 1\sigma$ percentiles. The dashed line in panel 1 is the best-fit curves to equation 11, which gives parameters $\Sigma_{crit} = 2800 \pm 100 M_{\odot} \text{pc}^{-2}$ and $\epsilon_{max} = 0.77 \pm 0.05$.

alistically, the diffuse gas would never form stars over the time-scale of interest, but would reduce the ϵ_{int} statistic if it were included in the gas mass sum. In our simulations, it is possible that there is a similar effect for the diffuse gas at the outer edges of the disk, as well as the gas which escapes through under-dense ‘chimneys’ between the dense sub-clouds within the disk.

We fit ϵ_{int} to the following two-parameter model:

$$\epsilon_{int} = \left(\frac{1}{\epsilon_{max}} + \frac{\Sigma_{crit}}{\Sigma_{tot,0}} \right)^{-1}, \quad (11)$$

which is equivalent to equation 9 in the limit $\Sigma_{tot,0} \ll \Sigma_{crit}$ but approaches ϵ_{max} as $\Sigma_{tot,0} \rightarrow \infty$. Performing an un-weighted fit on $\log \epsilon_{int}$, the best-fit parameters are $\Sigma_{crit} = 2800 \pm 100 M_{\odot} \text{pc}^{-2}$ and $\epsilon_{max} = 0.77 \pm 0.05$. The best-fit curve is plotted in panel 1 of Figure 4. This value of Σ_{crit} agrees well with our original estimate of Σ_{crit} in Section 2 from the median observed ϵ_{int} of Milky Way GMCs.

The residual R -dependence of ϵ_{int} is small, but is positively correlated with R . This may be explained by the built-in scales in ISM cooling and stellar feedback physics. It is expected that the thermal pressure of the warm ISM heated

to 10^4 K will have a greater proportional dynamical effect in the few clouds with escape velocities that do not greatly exceed 10 km s^{-1} . The time-scale of stellar evolution also introduces a scale into stellar feedback: at fixed $\Sigma_{tot,0}$, t_{ff} scales $\propto R^{\frac{1}{2}}$. Therefore, as R spans 2 dex, the time-scale of star formation spans an order of magnitude, so the timing of star formation relative to the stellar evolution within the formed stellar populations varies with R at fixed $\Sigma_{tot,0}$. Stellar evolution causes $\frac{\dot{P}_{\star}}{m_{\star}}$ to vary over time, so the effective strength of feedback that determines ϵ_{int} will be some function of the global star formation time-scale t_{ff} . The general trend is that of increasing SFE over longer dynamical times, indicating that the effective $\frac{\dot{P}_{\star}}{m_{\star}}$ decreases monotonically with time. This is *despite* the increasing relevance of supernovae in the simulations spanning longer time-scales: as massive stars die, the introduction of supernovae is not enough to make up for the loss of mechanical luminosity from radiation and stellar winds to maintain the initial $\frac{\dot{P}_{\star}}{m_{\star}}$.

In Figure 4, the compiled SFE statistics for GMC populations extracted from the parameter survey of full-scale galaxy simulations (Hopkins et al. 2012a) are also plotted

for comparison, and happen to be largely compatible with the fit. In light of this and the agreement with the observational estimate of Σ_{crit} , we may safely generalize these results from our contrived generic gas ball setup to clouds with actual GMC morphologies as they emerge from galactic gas dynamics. While the large-scale morphology and relative importances of shear and rotation may be different between our simulations and GMCs that emerge in galaxy simulations, the scaling of ϵ_{int} is an inevitable result that applies to self-gravitating gas cloud that can form stars. Therefore, equation 11 is useful as a general predictor of the ϵ_{int} of any star-forming gas cloud, provided that it is self-gravitating and it has some well-defined average surface density.

4.4 Duration of star formation and per-freefall SFE

As stated in the overview, star formation in all parameter survey simulations spans no more than $\sim 3t_{ff,0}$ (see Figures 2 and 3). Here we seek to quantify this statement more precisely. As a general-purpose measure of the duration of the starburst, we define the quantity T_{SF} , the stellar mass formed divided by the mass-weighted average star formation rate:

$$T_{SF} = \frac{M_{\star}}{\langle \dot{M}_{\star} \rangle} = \frac{M_{\star}^2}{\int (\dot{M}_{\star})^2 dt}. \quad (12)$$

This is a natural measure of the width of the peak in the star formation history (see Figures 2 and 3). It is also a useful proxy for the lifetime of the gas disk, as star formation largely begins once the gas has settled into a disk and halts once the disk is disrupted. The values of T_{SF} are tabulated in table 2. T_{SF} is insensitive to the small early and late tails of the star formation history, however, so in table 2 we also quote $T_{2\sigma}$, the time interval containing 95% of the star formation. This is generally only slightly more than T_{SF} , as most star formation occurs in a brief burst, and feedback is generally able to rapidly quench star formation.

In all simulations, $T_{SF} \sim t_{ff,0}$ (see table 2), so most of the star formation occurs within a single global freefall time. This agrees with our argument in Section 2: since $t_{ff,0}$ is longer than any other internal collapse time-scale, the disk should be able to form enough stars to reach the blowout stage within this time. This time constraint implies a tight relation between ϵ_{int} and ϵ_{ff} : if star formation is constrained to happen over N dynamical times, then $\epsilon_{ff} = \epsilon_{int}/N$.

This brings us to a very important subtlety of feedback-moderated star formation: while stellar feedback determines ϵ_{int} in a simple way through the force balance described in Section 2, it also determines ϵ_{ff} in an “instantaneous” sense, with “instantaneous” meaning over time-scales much longer than the dynamical time of the smallest resolved units of star formation. Since star formation is a process of hierarchical fragmentation from the largest cloud scale down to individual stars, the total star formation history is the sum of a hierarchy of many individual smaller and shorter star formation events, each of which has its ϵ_{int} determined by the local ratio of feedback and gravity. This results in an overall star formation rate which is moderated from the bottom up.

It is of limited usefulness to compare star formation time-scales to $t_{ff,0}$, at least when comparing with the

value of ϵ_{ff} in observed star-forming systems, as it requires knowledge of the more-diffuse initial conditions. The freefall time inferred for the gas disks as they would be observed during star formation would be something closer to $t_{ff,50}$, as defined in equation 6. Average values of $\epsilon_{ff,50} \equiv M_{\star}(t) t_{ff,50}(t) / M_{gas}(t)$ for each simulation can be found in columns 9 and 10 of table 2. In panel 1 of Figure 5 we plot $\epsilon_{ff,50}$ as a function of ϵ_{int} and confirm that there is a tight relation between two efficiencies. The best-fit power law to the relation has an exponent within 1σ of 1, so we propose a simple proportional relation:

$$\langle \epsilon_{ff,50} \rangle_t = 0.34 \epsilon_{int}, \quad (13)$$

where $\langle \epsilon_{ff,50} \rangle_t$ denotes the average observed value at a random point during the star formation history. The physical implication of this relation is that star formation in the simulations is indeed constrained to occur mainly within ~ 2 dynamical times, regardless of the relative strength of feedback and gravity, as was argued in Section 2.

The shape of the distribution of ϵ_{ff} , which we show in panel 2 of Figure 5, is also of interest. In general, the distribution is strongly peaked near ϵ_{int} , with only brief excursions above ϵ_{int} . The distribution is negatively skewed due to the early and late tails of the star formation history, which spread the distribution over several orders of magnitude. We also find that the *dispersion* in $\epsilon_{ff,50}$ has relatively little variation across simulations, having an average value of $\sigma_{\log \epsilon_{ff,50}} = 0.42$ dex with 0.06 dex spread. This intrinsic dispersion is the dispersion one would find when measuring ϵ_{ff} for a theoretical population of identical GMCs at different phases in their lifetimes. Because it is less than 0.5 dex, our simulated clouds would be quite likely to have an observationally-inferred SFR within an order of magnitude of their average SFR (ignoring practical considerations of SFR tracer lifetimes).

Given the surface densities of $\Sigma_{tot,0} \sim 100 - 300 M_{\odot} \text{pc}^{-2}$ typically measured in local GMCs (Larson 1981; Solomon et al. 1987; Bolatto et al. 2008), we may directly compare our results from the lower values of $\Sigma_{tot,0}$ that we have surveyed. $\sigma_{\log \epsilon_{ff,50}} = 0.42$ dex appears to be somewhat robust with respect to the scaling of $\Sigma_{tot,0}$, it is reasonable to assume its value remains the same at these slightly lower surface densities. For a population of Milky Way GMCs, Lee et al. (2016) measures a dispersion of $\sigma_{\log \epsilon_{ff}} = 0.91 \pm 0.22$ dex, while measuring $\sigma_{\log \epsilon_{int}} = 0.79 \pm 0.22$ dex. It is shown that the observed dispersion may be due to an intrinsically time-varying ϵ_{ff} , with a model giving $\sigma_{\log \epsilon_{ff},intrinsic} = 0.9$ dex providing the best fit to the observed distribution, more than twice as large as the intrinsic spread we have predicted. However, if $\epsilon_{ff} \propto \epsilon_{int}$, the observed dispersion $\sigma_{\log \epsilon_{ff},obs}$ will inherit a component from the variation in ϵ_{int} within the population:

$$\sigma_{\log \epsilon_{ff},obs}^2 = \sigma_{\log \epsilon_{int}}^2 + \sigma_{\log \epsilon_{ff},intrinsic}^2. \quad (14)$$

Taking $\sigma_{\log \epsilon_{ff},intrinsic} = 0.42$ dex from the simulations, and the observed value of $\sigma_{\log \epsilon_{ff}} = 0.79 \pm 0.22$ dex found in Lee et al. (2016), we obtain $\sigma_{\log \epsilon_{ff},obs} = 0.89$, in good agreement with the observed value. Thus, we propose that the observed distribution of per-freefall SFE in Milky Way GMCs may be fully accounted for by the combination of an intrinsic spread in ϵ_{ff} throughout the cloud lifetime and a proportional relationship between ϵ_{ff} and ϵ_{int} .

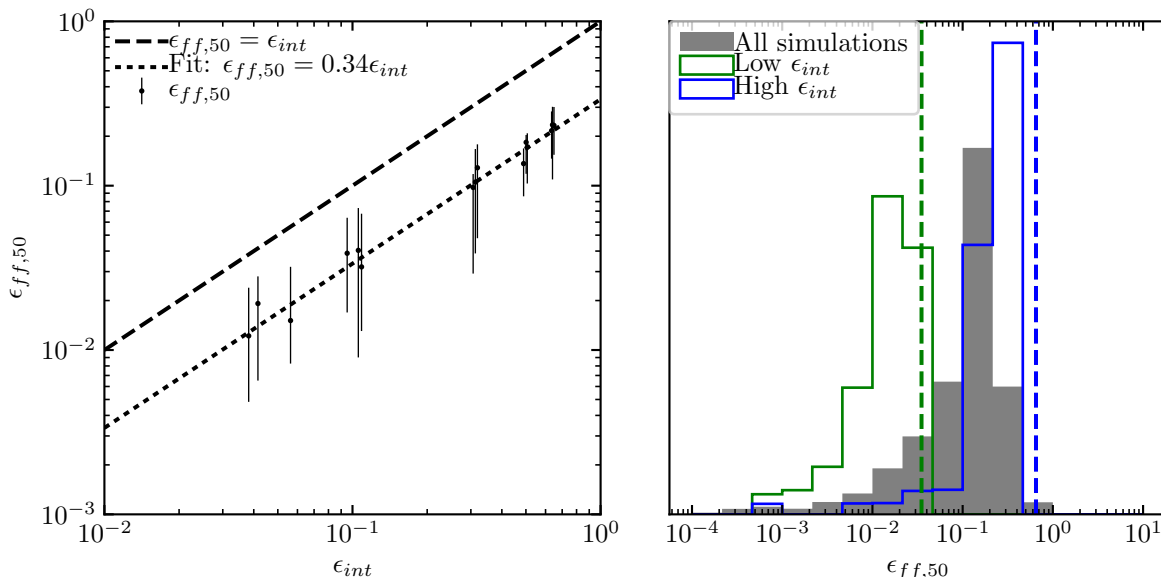


Figure 5. *Left:* Instantaneous per-freefall star formation efficiency $\epsilon_{ff,50} = \dot{M}_*(t) t_{ff,50}(t) / M_{gas}(t)$ (see equation 6) as a function of integrated star formation efficiency ϵ_{int} for all parameter survey simulations. The points represent the value of $\epsilon_{ff,50}$ averaged over all times where the SFR is nonzero. Error bars represent the $\pm 1\sigma$ percentiles of $\epsilon_{ff,50}$. The dashed line marks the line of equality between ϵ_{ff} and ϵ_{int} , and the dotted line indicates the best proportional fit. *Right:* Histograms of $\epsilon_{ff,50}$ for all parameter-survey simulations (grey), a highly-efficient ($\epsilon_{int} = 0.64$) run with $\Sigma_{tot,0} = 12700 M_{\odot} \text{pc}^{-2}$, $R = 50 \text{pc}$ (blue), and an inefficient ($\epsilon_{int} = 0.08$) run with $\Sigma_{tot,0} = 382 M_{\odot} \text{pc}^{-2}$, $R = 50 \text{pc}$ (green). The dashed lines indicate ϵ_{int} for the respective runs. Not surprisingly, $\epsilon_{ff,50}$ scales in proportion to ϵ_{int} , but it has considerable variation (~ 0.42 dex) throughout the star formation history of a single simulation. For Milky Way GMCs of surface density $\sim 100 M_{\odot} \text{pc}^{-2}$, we expect $\epsilon_{ff,50}$ to average to 0.01, in good agreement with observations.

5 DISCUSSION

5.1 Comparison with slow star formation

The scaling and saturation of ϵ_{ff} appears at first to be at odds with “slow” star formation, wherein it has been observed that $\epsilon_{ff} \sim 1\%$ universally, from Milky Way-like to ULIRG-like environments (Kennicutt 1998; Krumholz & McKee 2005; Krumholz & Tan 2007; Krumholz et al. 2012). In making this comparison, we emphasize that our prediction pertains to individual unstable clouds near virial equilibrium, and not to any significant patch of a galaxy that may contain GMCs in various states of formation and disruption, as well as the other phases of the ISM. In the latter case, it has been shown in Hopkins et al. (2014) and Orr et al. (2017) that the same physical models used in our simulations also robustly predict that $\epsilon_{ff,gal} \sim 1\%$ on galactic scales on average, despite assuming that $\epsilon_{ff} = 1$ on the smallest resolvable scales. The observations that most readily test our predictions are observations of the efficiency of individual nearby GMCs, for which we found good agreement in the previous section. Both our feedback-disrupted cloud model and turbulence-regulated slow star formation models predict the average value $\epsilon_{ff} \sim 1\%$ in Milky Way GMCs, albeit for completely different reasons. However, unlike our feedback-disrupted cloud model, turbulence-regulated models predicting locally slow star formation (Krumholz & McKee 2005; Hennebelle & Chabrier 2011) under-predict the observed scatter in ϵ_{ff} (Lee et al. 2016).

Direct comparison with observations in the $\Sigma_{gas} \sim 10^4 M_{\odot} \text{pc}^{-2}$, $\epsilon_{int} \sim 1$ regime of our simulations is less straightforward, as such clouds would only be found in ex-

treme environments that are not readily observable due to obscuration and resolution. Arp 220 is the nearest galaxy with gas surface density of this magnitude (Downes & Solomon 1998; Wilson et al. 2014), and observations have been thus far incapable of resolving individual clouds in its star-forming region. However, as mentioned in Section 1, the observed presence of young bound star clusters with a similar mass scale to the GMC may be a hallmark of highly efficient star formation in these environments (Keto et al. 2005; Murray 2011).

5.2 Comparison with other GMC disruption studies

Many numerical studies have been performed that are conceptually similar to the ones in this paper, following the collapse of an idealized turbulent cloud and the resulting star formation and feedback processes. It is useful to compare and contrast our predictions with these studies, in particular in cases where specific feedback mechanisms have been considered in greater detail.

Dale et al. (2012) ran a parameter study of feedback-disrupted clouds, considering only photoionization heating. We have found in tests that photoionization heating only is insufficient to disrupt a cloud with an escape velocity that is large compared to the sound speed $c_s \sim 10 \text{km s}^{-1}$ of photoionized gas. This agrees with the trend of Dale et al. (2012), which found order-unity ϵ_{int} in clouds with high escape velocity (Runs ‘X’ and ‘F’). Also, our $M = 10^4 M_{\odot} \text{pc}^{-2}$, $R = 5 \text{pc}$ has the same physical parameters as Run ‘J’ in Dale et al. (2012). This had $\epsilon_{int} = 0.04$, while the final stel-

lar mass in Run ‘J’ was 35% and rising at 3.5 Myr. We re-simulated this run with photoionization heating only and radiation pressure only, and the one with photoionization heating had a very similar star formation history and cloud morphology to Run ‘J’. The one with radiation pressure only had $\epsilon_{int} = 0.05$, very close to the full physics run. Radiation pressure is thus the primary feedback mechanism even in this region of parameter space where photoionization heating alone could still theoretically disrupt the cloud.

The radiation hydrodynamics star formation simulations of Raskutti et al. (2016) focus upon the effects of stellar feedback from the scattering of monochromatic photons at a high opacity corresponding to non-ionizing UV photons, using the radiation hydrodynamics code Hyperion (Skinner & Ostriker 2013). They overpredict the efficiency of their fiducial Milky Way-like GMC run by an order of magnitude, obtaining $\epsilon_{int} = 0.43$ for a cloud with $M = 5 \times 10^4 M_{\odot}$ and $R = 15$ pc, which has average surface density $70 M_{\odot} \text{pc}^{-2}$. Extrapolating our simulation results using equation 11 gives $\epsilon_{int} = 0.02$ for a cloud with these parameters, in much better agreement with observations Murray (2011); Lee et al. (2016). We have confirmed that $\epsilon_{int} \sim 0.02$ in a test run with otherwise similar initial conditions to Raskutti et al. (2016) and radiation pressure as the only feedback. This indicates a possible point of tension between the predictions of the LEBRON radiative transfer approximation (Hopkins et al. 2017) we use and Hyperion’s M_1 -closed Godunov scheme. Further work examining the fidelity of different radiation hydrodynamics methods in this problem is warranted, particularly with spatially-adaptive Lagrangian (e.g. Khatami & Hopkins (2017)) and AMR (e.g. Rosen et al. (2017)) RHD codes.

It should be noted that most star formation in the simulations mentioned in this section occurs within some fixed ($\sim 2 - 3$) number of global dynamical times, regardless of the final ϵ_{int} if the cloud is disrupted. This naturally leads to the linear relation between ϵ_{int} and ϵ_{ff} shown in Section 4.4, suggesting that this is a very general feature of the star formation-cloud disruption process, insensitive to the details of stellar feedback.

5.3 Bound star cluster formation

A population of bound star clusters is generally produced in all simulations. In the simulations with higher ϵ_{int} , the mass in bound clusters is an order-unity fraction of the total stellar mass. In the limit of low ϵ_{int} , we still do find some bound star clusters, but they generally represent a vanishingly-small fraction of the total stellar mass. These trends agree with observations, which suggest that the bound cluster formation efficiency is higher in high-density environments, yet only some small fraction in Milky-Way-like environments (Kruijssen 2012; Johnson et al. 2016).

In our simulations, star clusters form quite *generically* from dense, gravitationally unstable gas complexes, *despite the effects strong stellar feedback*, and *without* any contrived large-scale inflows or tidal shocks. As long as high enough surface density is reached, the disk can collapse into sub-clouds where the star formation efficiency is locally ~ 1 because the self-gravity is strong enough compared to feedback. Even if the overall star formation efficiency of the system is low, as is the case in the majority of GMCs in the Milky

Way and the local Universe, the inherent clustering of star formation produces over-dense substructures which can still have some bound remnant after the gas blowout. The production of bound star clusters with some non-zero efficiency even at lower Σ_{gas} is necessary to explain the presence of young bound star clusters in the Milky Way (see Portegies Zwart et al. (2010)). Detailed analysis of the mapping between GMC and bound cluster populations suggested by our simulations is deferred to a future paper.

The production of bound star clusters is generally observed in high-pressure environments (Elmegreen & Efremov 1997), where the pressure associated with the midplane of a galactic disk can be estimated as $P \sim G\Sigma_{gas}\Sigma_{tot}$. Thus it has been proposed that bound star cluster formation can be attributed to events wherein external pressure forces compress a molecular cloud, driving it to high density and producing a dense, bound remnant cluster (Keto et al. 2005). The scaling of star formation efficiency we have found motivates an alternative explanation: rather than the pressure itself causing cluster formation, both pressure and star formation efficiency are positively correlated with Σ_{gas} , so high-pressure regions would be expected to have high SFE due to the relative strength of feedback and gravity.

Further work is required to understand the mapping between galactic environments and the populations of bound star clusters they produce, providing the stepping stone between lower-resolution cosmological simulations and single-cluster dynamical studies. This development is necessary, in particular, for the theory of cosmological SMBH seed formation from runaway stellar mergers in dense clusters (see Portegies Zwart & McMillan (2002); Mouri & Taniguchi (2002); Gürkan et al. (2004); Devecchi & Volonteri (2009)). It would also allow a more self-consistent model of pairing and evolution of the population of massive ($\sim 60 M_{\odot}$) black hole binaries like the progenitor of GW150914 (Abbott et al. 2016); a significant fraction of these are expected to be found in bound star clusters (Rodriguez et al. 2015, 2016).

5.4 The nature of nuclear star formation

Our results here illustrate the claim of Torrey et al. (2016): *no equilibrium exists* for gas-rich nuclear disks with short dynamical times, and their dynamics have an inherently transient nature: they undergo rapid fragmentation followed by rapid gas expulsion. Star-forming nuclear disk calculations *must* account for stellar feedback in a way that is appropriate to their short time-scales, or else risk obtaining unphysical solutions. This caveat may very well limit the validity of isolated nuclear disk simulations that use a Springel & Hernquist (2003)-like effective-EOS ISM model and a slow sub-grid star formation law, both of which have been widely used in the field of galaxy simulations. For example, Hopkins & Quataert (2010) simulated circumnuclear disks of similar mass and radius to the ones in this paper, but in absence of the appropriate feedback physics the SFR of the disks was quite likely underestimated by at least an order of magnitude.

A robust result of our simulations is that both ϵ_{int} and ϵ_{ff} must saturate to ~ 1 at surface densities in excess of $10^4 M_{\odot} \text{pc}^{-2}$. Barring other unaccounted-for feedback physics (see Section 5.6), and neglecting environmental in-

teractions, we conclude that a gas-dominated cloud with $\Sigma_{gas} \gg 10^3 M_{\odot} \text{pc}^{-2}$ will convert nearly all of its gas to stars in a few crossing times. In this limit, we expect a result similar to our simulations: a population of massive star clusters will form, and will eventually merge into a single cluster because the high global SFE will allow the system to remain bound. If a relatively low-mass SMBH is present, it may sink to the centre of this cluster under dynamical friction. However, it is also possible that before the final nuclear cluster has formed, the SMBH and clusters effectively behave as a few- N -body system, which has chaotic behaviour and often results in the ejection of one or more members. Such ejections will prolong the time necessary for SMBH to form binary pairs in galaxy mergers, and may lower the resulting low-frequency gravitational wave background.

If star formation occurs near an SMBH, the gravity of the SMBH also contributes to the binding force on the gas. If we re-derive 9 and consider only the force of gravity of the SMBH on the gas, we obtain a lower bound for the integrated SFE of a gas disk of radius R around a black hole of mass M_{BH} :

$$\epsilon_{int} \geq \left(1 + \frac{\pi R^2 \Sigma_{crit}}{M_{BH}}\right)^{-1}. \quad (15)$$

This assumes that the gas is not somehow being prevented from forming stars by AGN feedback and that the dynamical effect of the black hole upon the gas flow does not slow star formation enough to make the gas consumption time longer than ~ 10 Myr. The characteristic radius at which ϵ_{int} saturates to ~ 1 is then:

$$R_{SF} \sim \sqrt{M_{BH}/2\pi\Sigma_{crit}} = 6 \text{ pc} \left(\frac{M_{BH}}{10^6 M_{\odot}}\right)^{\frac{1}{2}}, \quad (16)$$

using $\Sigma_{crit} = 2800 M_{\odot} \text{pc}^{-2}$.

Under these assumptions, the in-situ formation of a nuclear star cluster could proceed as follows: if enough low-angular momentum gas falls within R_{SF} of an SMBH to become gravitationally unstable, it will be rapidly consumed by star formation, leaving behind a nuclear star cluster and little remaining gas. The fiducial value 6 pc derived here does lie in the range of effective radii of nuclear star clusters found in several different types of galaxies (see Hopkins et al. (2010) and references therein).

Such efficient star formation near black holes may have drastic implications for the ability of gas from the galactic disk to be accreted onto a central SMBH, as the gas may fragment into stars before reaching the hole within a few dynamical times, at which point it can no longer lose angular momentum efficiently. This contrasts greatly with models which assume star formation must be slow ($\epsilon_{ff} \sim 1\%$) all the way down to the black hole; in this case, a steady supply of gas can reach the black hole even with modest torques, as gas has ~ 100 dynamical times to lose its angular momentum before being converted to stars. As such, it is important that studies of AGN accretion on $\sim \text{pc}$ and smaller scales consider the physics of the multiphase ISM and star formation in some detail.

5.5 Absence of metal-enriched supermassive direct-collapse objects

These simulations were originally conceived as an attempt to reproduce the mechanism for direct-collapse supermassive black hole formation simulated in Mayer et al. (2010) and Mayer et al. (2015) with a more realistic approach to cooling and star formation. To summarize, these works propose that in the gas-rich nuclear disk resulting from a galaxy merger, fragmentation can be suppressed by some combination of turbulence and suppression of cooling due to optical thickness, enabling accretion onto a supermassive quasi-star even for ISM with solar metal abundances. To avoid over-cooling in optically thick regions, we implemented the optically-thick cooling approximation of Rafikov (2007) so as to interpolate between the optically-thin and -thick cooling regimes where appropriate. In previous tests we also chose a rather high (10^7cm^{-3}) density threshold for star formation and allowed star formation only when the local Jeans mass is $< 10^3 M_{\odot}$, so as to prevent premature conversion of gas particles into star particles where they may otherwise form a supermassive object. Our simulations reach comparable optical depths and turbulent velocity dispersions to the nuclear disks in the Mayer simulations, however we report no formation of direct-collapse objects. In numerical experiments, we have only been able to produce anything resembling a supermassive quasi-star if we implement a temperature floor of 10^4K and slow the local star formation rate $\dot{\rho}_{\star}$ to 1% of the usual value. As these are similar to the choices made for Mayer et al. (2010) and Mayer et al. (2015), it seems that metal-enriched direct-collapse object formation is a numerical artifact of slow subgrid star formation and a lack of low-temperature cooling. Our conclusions agree with those obtained by Ferrara et al. (2013) using a one-dimensional disk model: if realistic low-temperature cooling is accounted for, the cooling time in the metal-enriched ISM is invariably too short to suppress fragmentation down to the scales required to directly form a supermassive object.

5.6 Feedback physics uncertainties

Most of what is known about the effects of stellar feedback on GMC scales has been learned from observations of star-forming complexes within the Milky Way, and even then the true efficiencies of many feedback mechanisms acting in Milky Way-like environments are still loosely constrained, to say nothing of generalizing these mechanisms to ULIRG-like environments. Here we list uncertainties in the strength of feedback which could conceivably affect our results:

5.6.1 The Initial Mass Function

Throughout this work, we have assumed that the initial stellar mass function, and hence $\dot{P}_{\star}/m_{\star}$, is independent of the environment of star formation. If the IMF were to become more top-heavy in environments of high surface density, $\dot{P}_{\star}/m_{\star}$ would increase, and as our simulations have shown, this is the quantity to which our results are most sensitive. Supposing that $\frac{\dot{P}_{\star}}{m_{\star}}$ did scale at least linearly with Σ_{gas} due to enhanced type O star production, this would limit the maximum star formation efficiency. There is some observational

evidence of a dearth of low-mass stars in dense nuclear environments (Smith & Gallagher 2001; Bartko et al. 2010), however such observations can be subject to significant sampling bias because the time-scale for mass segregation is short in dense systems. For this reason and others, Bastian et al. (2010) concluded that current observations were still largely consistent with a universal IMF.

5.6.2 Infrared radiation pressure

Radiation pressure plays an important role in the feedback budget many of our simulations; even in cases where the final gas blowout is ultimately due to SNe, radiation helps prevent an initial runaway of the SFE before SNe start to occur. We have found that ϵ_{int} saturates to a value close to 1 as surface density becomes large, however Murray et al. (2010) argued that the IR opacity of dust grains should limit the saturation point of ϵ_{int} for gas with solar abundances, as radiation pressure in the optically thick regime is the only force of feedback which can conceivably scale as fast as the gas self-gravity. By this argument, the saturation SFE ϵ_{int}^{max} is expected to scale $\sim (\kappa_{IR}\Sigma_{crit})^{-1}$, which takes a value of $\sim \frac{1}{2}$ for gas with solar metal abundances. However, in a realistic, 3-dimensional scenario where hydrodynamics is coupled to the radiation field in an inhomogeneous ISM, it is actually unlikely that radiation pressure can achieve the whole “ τ_{IR} boost”, as photons will have a tendency to leak out of the most optically thin lines of sight. Radiation hydrodynamics studies on this problem are ongoing (see Davis et al. (2014); Skinner & Ostriker (2015); Zhang & Davis (2017)).

6 SUMMARY

We have performed a parameter study of 3D multi-physics MHD simulations of star-forming gas disks with initial parameters spanning two orders of magnitude in surface density and in spatial scale, including the physics of supernovae, stellar winds, radiation pressure, and photoionization heating. Due to the generality of the simulation setup, we have been able to study the nature of star formation in gas-rich environments in general, including nuclear starbursts and GMCs. Our main findings are as follows:

- In any bound, gas-rich star-forming cloud with short (~ 10 Myr or less) dynamical time, star formation proceeds until it causes an inevitable gas blowout, with the final SFE determined mainly by the balance of feedback and gravitation, with other physical mechanisms having secondary importance.
- The integrated SFE ϵ_{int} of such a system scales strongly with the initial gas surface density $\Sigma_{tot,0}$ with weak dependence upon other parameters, and saturates to a value ~ 1 at adequately high surface density, despite the effects of strong feedback. We find surprisingly good agreement with analytic derivations of ϵ_{int} which take the form of equation 9 (Fall et al. 2010; Murray et al. 2010; Dekel & Krumholz 2013; Thompson & Krumholz 2016). The agreement across different spatial scales is particularly surprising, given that our parameter space bridges distinct time-scale regions where radiation pressure (< 3 Myr) and SN explosions (> 3 Myr) dominate the feedback budget.

- We find a proportional relation between the integrated SFE ϵ_{int} and the per-freefall SFE ϵ_{ff} (equation 13) for self-gravitating clouds, essentially because the clouds always produce enough stars to self-destruct within $\sim 2 - 3$ dynamical times. ϵ_{ff} is determined only initially by such details as cooling and magnetic fields, and will inevitably grow until moderated by stellar feedback. The observed ϵ_{ff} distribution for Milky Way GMCs can be accounted for by combining the spread from this relation and a modest intrinsic spread due to the time-varying SFE of a single cloud. The variation in ϵ_{ff} is at odds with a universal slow star formation ($\epsilon_{ff} \sim 1\%$) law when applied to individual clouds, but the same physics used in this study recover the $\epsilon_{ff,gal} \sim 1\%$ relation in cosmological simulations (Hopkins et al. 2014, 2017).

- Bound star cluster formation occurs to some extent in every simulation, suggesting that it is a generic result of star formation even with “strong” stellar feedback. This is even so for clouds which have an overall SFE significantly less than 1, although the mass fraction in bound star clusters becomes small in this case, similar to what is observed in the Local Group (Portegies Zwart et al. 2010; Kruijssen 2012; Johnson et al. 2016). Even when the global SFE is small, it can still be high on smaller scales, allowing clusters to remain bound after gas is expelled. In future work we will present more detailed results on star cluster formation and structure, the cluster formation efficiency, and the dependencies of the cluster mass and size functions.

ACKNOWLEDGMENTS

We thank Dávid Guszejnov, Chris Hayward, Matthew Orr and Andrew Wetzel for helpful comments and critique. We also thank the anonymous referee for highly comprehensive and helpful feedback. Support for PFH and MG was provided by an Alfred P. Sloan Research Fellowship, NASA ATP Grant NNX14AH35G and NSF Collaborative Research Grant #1411920 and CAREER grant #1455342. Numerical calculations were run on the Caltech computer cluster ‘Zwicky’ (NSF MRI award #PHY-0960291) and allocation TG-AST130039 granted by the Extreme Science and Engineering Discovery Environment (XSEDE) supported by the NSF.

REFERENCES

- Abbott B. P., et al., 2016, *Physical Review Letters*, **116**, 061102
 Agertz O., Kravtsov A. V., Leitner S. N., Gnedin N. Y., 2013, *ApJ*, **770**, 25
 Bartko H., et al., 2010, *ApJ*, **708**, 834
 Bastian N., Covey K. R., Meyer M. R., 2010, *ARA&A*, **48**, 339
 Bastian N., et al., 2012, *MNRAS*, **419**, 2606
 Bate M. R., Bonnell I. A., Price N. M., 1995, *MNRAS*, **277**, 362
 Bolatto A. D., Leroy A. K., Rosolowsky E., Walter F., Blitz L., 2008, *ApJ*, **686**, 948
 Bryant P. M., Scoville N. Z., 1999, *AJ*, **117**, 2632
 Collins D. C., Kritsuk A. G., Padoan P., Li H., Xu H., Ustyugov S. D., Norman M. L., 2012, *ApJ*, **750**, 13
 Dale J. E., Ercolano B., Bonnell I. A., 2012, *MNRAS*, **424**, 377
 Davis S. W., Jiang Y.-F., Stone J. M., Murray N., 2014, *ApJ*, **796**, 107
 Dekel A., Krumholz M. R., 2013, *MNRAS*, **432**, 455
 Devecchi B., Volonteri M., 2009, *ApJ*, **694**, 302
 Downes D., Solomon P. M., 1998, *ApJ*, **507**, 615

- Elmegreen B. G., Efremov Y. N., 1997, *ApJ*, **480**, 235
- Fall S. M., Krumholz M. R., Matzner C. D., 2010, *ApJ*, **710**, L142
- Faucher-Giguère C.-A., Quataert E., Hopkins P. F., 2013, *MNRAS*, **433**, 1970
- Federrath C., Klessen R. S., 2012, *ApJ*, **761**, 156
- Federrath C., Schober J., Bovino S., Schleicher D. R. G., 2014, *ApJ*, **797**, L19
- Ferrara A., Haardt F., Salvaterra R., 2013, *MNRAS*, **434**, 2600
- Gürkan M. A., Freitag M., Rasio F. A., 2004, *ApJ*, **604**, 632
- Hennebelle P., Chabrier G., 2011, *ApJ*, **743**, L29
- Hills J. G., 1980, *ApJ*, **235**, 986
- Hollyhead K., Bastian N., Adamo A., Silva-Villa E., Dale J., Ryon J. E., Gazak Z., 2015, *MNRAS*, **449**, 1106
- Hopkins P. F., 2015, *MNRAS*, **450**, 53
- Hopkins P. F., Conroy C., 2015, preprint, ([arXiv:1512.03834](https://arxiv.org/abs/1512.03834))
- Hopkins P. F., Quataert E., 2010, *MNRAS*, **407**, 1529
- Hopkins P. F., Raives M. J., 2016, *MNRAS*, **455**, 51
- Hopkins P. F., Murray N., Quataert E., Thompson T. A., 2010, *MNRAS*, **401**, L19
- Hopkins P. F., Quataert E., Murray N., 2011, *MNRAS*, **417**, 950
- Hopkins P. F., Quataert E., Murray N., 2012a, *MNRAS*, **421**, 3488
- Hopkins P. F., Quataert E., Murray N., 2012b, *MNRAS*, **421**, 3522
- Hopkins P. F., Narayanan D., Murray N., 2013, *MNRAS*, **432**, 2647
- Hopkins P. F., Keres D., Onorbe J., Faucher-Giguère C.-A., Quataert E., Murray N., Bullock J. S., 2014, *MNRAS*, **445**, 581
- Hopkins P. F., Torrey P., Faucher-Giguère C.-A., Quataert E., Murray N., 2016, *MNRAS*, **458**, 816
- Hopkins P. F., et al., 2017, preprint, ([arXiv:1702.06148](https://arxiv.org/abs/1702.06148))
- Johnson L. C., et al., 2016, *ApJ*, **827**, 33
- Kennicutt Jr. R. C., 1998, *ApJ*, **498**, 541
- Keto E., Ho L. C., Lo K.-Y., 2005, *ApJ*, **635**, 1062
- Khatami D., Hopkins P. F., 2017, *MNRAS*, in prep.
- Kim C.-G., Ostriker E. C., 2015, *ApJ*, **802**, 99
- Kritsuk A. G., Norman M. L., Wagner R., 2011, *ApJ*, **727**, L20
- Kroupa P., 2002, *Science*, **295**, 82
- Kruijssen J. M. D., 2012, *MNRAS*, **426**, 3008
- Kruijssen J. M. D., Maschberger T., Moeckel N., Clarke C. J., Bastian N., Bonnell I. A., 2012, *MNRAS*, **419**, 841
- Krumholz M. R., Gnedin N. Y., 2011, *ApJ*, **729**, 36
- Krumholz M. R., McKee C. F., 2005, *ApJ*, **630**, 250
- Krumholz M. R., Tan J. C., 2007, *ApJ*, **654**, 304
- Krumholz M. R., Klein R. I., McKee C. F., 2011, *ApJ*, **740**, 74
- Krumholz M. R., Dekel A., McKee C. F., 2012, *ApJ*, **745**, 69
- Larson R. B., 1981, *MNRAS*, **194**, 809
- Lee E. J., Miville-Deschênes M.-A., Murray N. W., 2016, *ApJ*, **833**, 229
- Martizzi D., Faucher-Giguère C.-A., Quataert E., 2015, *MNRAS*, **450**, 504
- Mayer L., Kazantzidis S., Escala A., Callegari S., 2010, *Nature*, **466**, 1082
- Mayer L., Fiacconi D., Bonoli S., Quinn T., Roškar R., Shen S., Wadsley J., 2015, *ApJ*, **810**, 51
- McCraday N., Graham J. R., 2007, *ApJ*, **663**, 844
- Mouri H., Taniguchi Y., 2002, *ApJ*, **566**, L17
- Murray N., 2011, *ApJ*, **729**, 133
- Murray N., Quataert E., Thompson T. A., 2010, *ApJ*, **709**, 191
- Myers A. T., Klein R. I., Krumholz M. R., McKee C. F., 2014, *MNRAS*, **439**, 3420
- Nordlund Å. K., Padoan P., 1999, in Franco J., Carramiñana A., eds, *Interstellar Turbulence*. p. 218 ([arXiv:astro-ph/9810074](https://arxiv.org/abs/astro-ph/9810074))
- Orr M., et al., 2017, preprint, ([arXiv:1701.01788](https://arxiv.org/abs/1701.01788))
- Ostriker E. C., Shetty R., 2011, *ApJ*, **731**, 41
- Padoan P., Nordlund A., Jones B. J. T., 1997, *MNRAS*, **288**, 145
- Portegies Zwart S. F., McMillan S. L. W., 2002, *ApJ*, **576**, 899
- Portegies Zwart S. F., McMillan S. L. W., Gieles M., 2010, *ARA&A*, **48**, 431
- Rafikov R. R., 2007, *ApJ*, **662**, 642
- Raskutti S., Ostriker E. C., Skinner M. A., 2016, preprint, ([arXiv:1608.04469](https://arxiv.org/abs/1608.04469))
- Rees M. J., 1976, *MNRAS*, **176**, 483
- Richings A. J., Schaye J., Oppenheimer B. D., 2014a, *MNRAS*, **440**, 3349
- Richings A. J., Schaye J., Oppenheimer B. D., 2014b, *MNRAS*, **442**, 2780
- Rodriguez C. L., Morscher M., Pattabiraman B., Chatterjee S., Haster C.-J., Rasio F. A., 2015, *Physical Review Letters*, **115**, 051101
- Rodriguez C. L., Chatterjee S., Rasio F. A., 2016, *Phys. Rev. D*, **93**, 084029
- Rosen A. L., Krumholz M. R., Oishi J. S., Lee A. T., Klein R. I., 2017, *Journal of Computational Physics*, **330**, 924
- Ryon J. E., et al., 2015, *MNRAS*, **452**, 525
- Saitoh T. R., Daisaka H., Kokubo E., Makino J., Okamoto T., Tomisaka K., Wada K., Yoshida N., 2008, *PASJ*, **60**, 667
- Skinner M. A., Ostriker E. C., 2013, *ApJS*, **206**, 21
- Skinner M. A., Ostriker E. C., 2015, *ApJ*, **809**, 187
- Smith L. J., Gallagher J. S., 2001, *MNRAS*, **326**, 1027
- Solomon P. M., Rivolo A. R., Barrett J., Yahil A., 1987, *ApJ*, **319**, 730
- Springel V., 2005, *MNRAS*, **364**, 1105
- Springel V., 2010, *MNRAS*, **401**, 791
- Springel V., Hernquist L., 2003, *MNRAS*, **339**, 289
- Stone J. M., Gardiner T. A., Teuben P., Hawley J. F., Simon J. B., 2008, *ApJS*, **178**, 137
- Su K.-Y., Hopkins P. F., Hayward C. C., Faucher-Giguère C.-A., Keres D., Ma X., Robles V. H., 2016, preprint, ([arXiv:1607.05274](https://arxiv.org/abs/1607.05274))
- Thompson T. A., Krumholz M. R., 2016, *MNRAS*, **455**, 334
- Thompson T. A., Quataert E., Murray N., 2005, *ApJ*, **630**, 167
- Torrey P., Hopkins P. F., Faucher-Giguère C.-A., Vogelsberger M., Quataert E., Keres D., Murray N., 2016, preprint, ([arXiv:1601.07186](https://arxiv.org/abs/1601.07186))
- Troland T. H., Crutcher R. M., 2008, *ApJ*, **680**, 457
- Vazquez-Semadeni E., 1994, *ApJ*, **423**, 681
- Vink J. S., de Koter A., Lamers H. J. G. L. M., 2001, *A&A*, **369**, 574
- Wilson C. D., Harris W. E., Longden R., Scoville N. Z., 2006, *ApJ*, **641**, 763
- Wilson C. D., Rangwala N., Glenn J., Maloney P. R., Spinoglio L., Pereira-Santaella M., 2014, *ApJ*, **789**, L36
- Yeast-Hull T. M., Gallagher J. S., Zweibel E. G., 2016, *MNRAS*, **457**, L29
- Zhang D., Davis S. W., 2017, *ApJ*, **839**, 54

APPENDIX A: CONVERGENCE AND CONSISTENCY TESTS

The methods for cooling, star formation and feedback used in this paper have been tested in previous studies of galactic-scale simulations resolving spatial scales of ~ 1 pc and masses $> 10^3 M_{\odot}$. However, their behaviour at the higher resolutions of these simulations has been much less well-studied. It is therefore necessary to determine how the simulation behaviour depends (1) upon mass and spatial resolution, (2) upon the particular random seeding in the initial conditions and (3) upon the particular physics included and parameters chosen. Because the star formation histories (SFH) are the main data of interest, we shall focus on the effects of

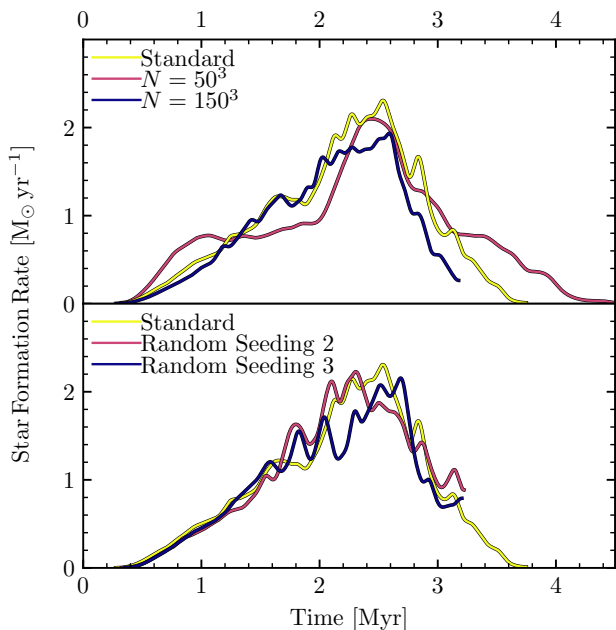


Figure A1. Star formation histories of test runs with parameters $M = 10^7 M_{\odot}$ and $R = 50$ pc. *Top:* Convergence tests with particle number varied from 50^3 to 200^3 . *Bottom:* Consistency tests using 3 different random seeds for the initial perturbations.

these choices on the SFH as a proxy for the behaviour of the simulation as a whole.

We choose the parameters $R = 50$ pc, $M = 10^7 M_{\odot}$ as the point in parameter space at which to investigate these questions. Because all runs are qualitatively identical with only differences in numerical scalings, the conclusions drawn for these parameters should apply across our parameter space, obviating the need to perform the tests at all points. We vary the particle number from 50^3 to 150^3 to isolate resolution effects. Because we use adaptive softening, the effective force resolution naturally follows mass resolution with no need for manual tuning. To assess the effect of the random velocity seeding, we compare runs from 3 random realizations at the standard resolution and with standard physics.

From the first panel of Figure A1 it is evident that mass resolution does have certain systematic effects upon the computed SFH: in particular, low-resolution runs have a SFR which is greater at early times. This is an artifact the cutoff in the turbulent length scale that can be followed before the turbulent Jeans mass is no longer resolved. A gas structure that is well-resolved and supported against its self-gravity by internal motions at high resolution may not be considered so if down-sampled to low resolution where it consists only of a few particles. Thus, in the absence of any feedback moderation, as is the case at early times, the SFR will rise sooner at low resolution. While this resolution effect is conspicuous, it apparently does not have a strong effect upon the integrated SFE.

The variation in SFE due to resolution is in fact comparable to the variation arising from different random seedings at fixed resolution, visible in panel 2 of Figure 2. In both cases, the mass of gas converted to stars varies only by $\sim 1\%$

between runs. We therefore conclude that the star formation efficiencies computed as the central result of this study are consistent between runs with the same physical parameters, at least to the level that can be expected from a highly nonlinear numerical simulation.

As discussed in the main text, our results concerning star formation efficiency can be understood in terms of simple force balance considerations. As such, it is not surprising that the SFE should converge rapidly and be robust with respect to perturbations.